



PCCP

How great is the stabilization of crowded polyphenylbiphenyls by London dispersion?

Journal:	<i>Physical Chemistry Chemical Physics</i>
Manuscript ID	CP-ART-10-2022-005085.R2
Article Type:	Paper
Date Submitted by the Author:	26-Mar-2023
Complete List of Authors:	Reis Alves Costa Lima, Carlos Filipe; Universidade do Porto Faculdade de Ciencias, Química e Bioquímica Mague, Joel; Tulane University, Chemistry Du, Yuchen; Tulane University, Chemistry Pascal, Robert; Tulane University, Chemistry Santos, Luis; Universidade do Porto, Quimica e Bioquimica

SCHOLARONE™
Manuscripts

How great is the stabilization of crowded polyphenylbiphenyls by London dispersion?

Carlos F. R. A. C. Lima,^a Joel T. Mague,^b Yuchen Du,^b
Robert A. Pascal, Jr.,^b and Luís M. N. B. F. Santos^{*a}

Department of Chemistry, Tulane University, New Orleans, LA 70118, USA

and

CIQUP, Institute of Molecular Sciences (IMS), Departamento de Química e Bioquímica,
Faculdade de Ciências, Universidade do Porto, rua do Campo Alegre s/n 4169-007 Porto,
Portugal

^aUniversidade do Porto

^bTulane University

Abstract

Decaphenylbiphenyl (**1**) and 2,2',4,4',6,6'-hexaphenylbiphenyl (**2**) are bulky molecules expected to be greatly destabilized by steric crowding. Herein, through a combined experimental and computational approach, we evaluate the molecular energetics of crowded biphenyls. This is complemented by the study of phase equilibria for **1** and **2**. Compound **1** shows a rich phase behavior, displaying an unusual interconversion between two polymorphs. Surprisingly, the polymorph with distorted molecules of C_1 symmetry is found to have the highest melting point and to be the one that is preferentially formed. The thermodynamic results also indicate that the polymorph displaying the more regular D_2 molecular geometry has larger heat capacity and is probably the more stable at lower temperatures. The melting and sublimation data clearly reveal the weakening of cohesive forces in crowded biphenyls due to the lower molecular surface area. The experimental quantification of the intramolecular interactions in **1** and **2** indicated, using homodesmotic reactions, a molecular stabilization of about $30 \text{ kJ}\cdot\text{mol}^{-1}$. We attribute the origin of this stabilization in both compounds to the existence of two parallel-displaced $\pi\cdots\pi$ interactions between the *ortho*-phenyl substituents on each side of the central biphenyl. Computational calculations with dispersion-corrected DFT methods underestimate the stabilization in **1**, unless the steric crowding is well balanced in a homodesmotic scheme. This work demonstrates that London dispersion forces are important in crowded aromatic systems, making these molecules considerably more stable than previously thought.

Introduction

Perphenyl arenes are sterically congested aromatic hydrocarbons whose molecular structure and stability challenge common perceptions in Chemistry.¹⁻⁸ These crowded molecules often release congestion by distortion from planarity, adopting twisted and chiral molecular geometries. That is the case, for example, for decaphenylanthracene,⁶ decaphenylphenanthrene,⁷ and dodecaphenyltetracene.⁸ Dodecaphenyltetracene was one of the standout molecules of 2019, according to *C&EN*, for being the longest, most twisted perphenylacene yet synthesized.^{8,9} Apart from the synthetic challenge to build these molecules, polyphenylene cores with congested aromatic rings (e.g. hexaphenylbenzene, rubrene) are archetypes for many structures with impact in organic electronics and nanochemistry.¹⁰⁻¹³

Decaphenylbiphenyl was first synthesized in 1965,¹ and reveals itself as an atypical member of the family of perphenyl arenes. To all appearances, decaphenylbiphenyl¹ (**1**, Equation 1, Table 1) is a strained molecule. Its X-ray structure² reveals numerous nonstandard bond angles and torsion angles, chiefly due to steric conflicts among the four phenyl groups *ortho* to the central bond, as well as the bending of one of the central biphenyl rings into a shallow boat conformation. The observed distortions must have an energetic cost, but precisely how strained is decaphenylbiphenyl?

Having substantial volumes of π electron density and being highly polarizable molecules, perphenyl arenes are prone to establish significant London dispersive interactions. Although relatively weak, London forces become significant in large polarizable systems, to the point that they can contribute to the stabilization of bulky molecules or molecules with bulky substituents.¹⁴⁻¹⁷ In the recent review of Mears and Power,¹⁴ the authors recognize the importance of intramolecular London dispersion forces in the properties of crowded metal catalysts and their consequent impact on catalyst design. The implications of London dispersion in crystal packing^{18,19} and protein folding^{20,21} cannot be ignored. While analyzing the impact of secondary forces, like aromatic interactions, in protein folding, Newberry and Raines emphasize that “weak but abundant interactions are likely to make greater overall contributions to protein

folding, particularly at the level of secondary structure.”²¹ Although ubiquitous in Nature, the accurate computation of dispersion forces is still challenging, mostly due to the significant amount of correlation energy involved and the relative weak and smooth potentials associated to such interactions.^{22,23} As stated by Wagner and Schreiner,¹⁶ we build on the idea that the quantitation of dispersion energy will improve our ability to design sophisticated molecular structures and better catalysts. Because of their very low polarity, dispersion forces are one of the major components of the intermolecular and intramolecular interaction potentials in perphenyl arenes. This makes such molecules a suitable probe for evaluating and quantifying London dispersion, and they also test the accuracy of computational methods.

We recently described the synthesis of several crowded biaryls,³ and in that paper, we estimated the strain in compound **1** by calculating the energy of the homodesmotic reaction shown in Equation 1. Pentaphenylbenzene (**3**) and biphenyl (**4**) are at least relatively unstrained, benzene (**5**) is unstrained, and none of the bonding in these molecules is unusual; thus, the energy for Equation 1 should be a fair approximation of the strain energy of **1**. At the B3PW91/6-311G(d,p) level^{24,25} of theory, the zero-point energy-corrected energy of this reaction [$\Delta(E+ZPE)$] is +95.9 kJ·mol⁻¹ (+22.9 kcal·mol⁻¹), a reasonable value when one considers the distortions observed in compound **1**. However, conventional DFT functionals such as B3PW91 do not account for London dispersion, and when the calculations are performed with the same basis set, but using the highly rated,²⁶ dispersion-corrected functionals M052X-D3 and PW6B95-D3(BJ),²⁷⁻³⁰ the reaction energy drops to -9.4 kJ·mol⁻¹ and -14.3 kJ·mol⁻¹, respectively. These calculations indicate that the formation of decaphenylbiphenyl from two pentaphenylbenzenes is *more favorable* than the formation of biphenyl from two benzenes, at least in the gas phase. Can this be true? Can the attraction of the four central phenyl groups in compound **1**, due to London dispersion, more than compensate for the costs of steric conflict and molecular distortion in **1**?

Herein we report additional DFT calculations bearing on this matter, as well as similar calculations for the closely related 2,2',4,4',6,6'-hexaphenylbiphenyl (**2**, Equation 2, Table 1). More significantly, we report the experimental gas-phase enthalpies of formation for compounds

1 and **2**. Combined with the literature experimental thermochemical data for the other molecules in Equations 1 and 2,³¹⁻³⁵ the results provide a direct experimental quantification of molecular energetics of heavily crowded biphenyls. Moreover, they can be used to test the accuracy of modern DFT calculations using molecules that are much larger than those typically employed as experimental and computational references for such methods.

How great is destabilization (or stabilization) of a very crowded molecule like decaphenylbiphenyl? How accurately do common methods in computational chemistry describe such extreme cases of molecular crowding? Does a distorted structure necessarily imply the existence of strain or steric conflict, or does it instead hint at a different balance of the usual attractive forces in molecules? Our findings question the usual perceptions of strain in organic molecules. The results indicate that stabilization due to London dispersion in such crowded aromatic systems is larger than previously anticipated, and, if anything, that current dispersion-corrected DFT methods underestimate the magnitude of these stabilizing interactions.

Results and Discussion

Computational studies. Table 1 summarizes a series of calculations for Equations 1 and 2. The full computational data, including the optimized atomic coordinates and the tabulation of the absolute energies for each molecule in the equations, are found in the ESI†. The data were calculated using both the 6-311G(d,p) and 6-311++G(2d,p) basis sets²⁵ for all three DFT methods previously mentioned [B3PW91, M052X-D3 and PW6B95-D3(BJ)]. The latter basis set, which includes diffuse functions on both carbon and hydrogen, was chosen to minimize the effects of basis set superposition error. However, the results are very similar with both basis sets, clearly indicating that the observed differences between the methods are chiefly due to the choice of functional. For comparison with experimental data, the gas-phase enthalpies of reaction are the quantities of interest. These are provided directly when a frequency calculation is performed in Gaussian 16,³⁶ and it can be seen from Table 1 that, for these reactions, the calculated energies and enthalpies of reaction are scarcely different. For all methods, the

enthalpies of reaction for Equation 2 were calculated to be slightly lower (more negative) than for Equation 1, and for both equations, the two dispersion-corrected DFT methods gave much lower enthalpies of reaction than found with B3PW91.

Table 1. Computationally Estimated Strain in Crowded Biphenyls.

(Eq. 1)

Level	ΔE (kJ·mol ⁻¹)	$\Delta(E+ZPE)$ (kJ·mol ⁻¹)	ΔH_{298} (kJ·mol ⁻¹)
B3PW91/6-311G(d,p)	+98.1 ^a	+95.9 ^a	+96.9
M052X-D3/6-311G(d,p)	-6.1 ^a	-9.4 ^a	-8.2
PW6B95-D3(BJ)/6-311G(d,p)	-14.5 ^a	-14.3 ^a	-14.3
B3PW91/6-311++G(2d,p)	+103.9	+93.9	+94.9
M052X-D3/6-311++G(2d,p)	+3.4	+0.3	+1.5
PW6B95-D3(BJ)/6-311++G(2d,p)	-4.7	-6.1	-5.4

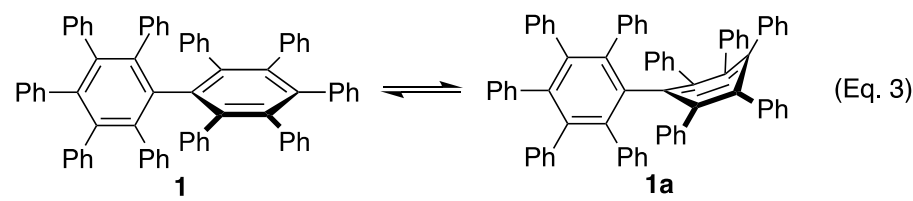
(Eq. 2)

Level	ΔE (kJ·mol ⁻¹)	$\Delta(E+ZPE)$ (kJ·mol ⁻¹)	ΔH_{298} (kJ·mol ⁻¹)
B3PW91/6-311G(d,p)	+65.5	+63.8	+65.2
M052X-D3/6-311G(d,p)	-15.6	-15.6	-15.1
PW6B95-D3(BJ)/6-311G(d,p)	-21.4	-23.8	-22.4
B3PW91/6-311++G(2d,p)	+70.5	+69.0	+70.4
M052X-D3/6-311++G(2d,p)	-5.6	-6.5	-5.6
PW6B95-D3(BJ)/6-311++G(2d,p)	-12.2	-11.8	-11.8

^a Ref. 3.

The identity of the preferred conformation of decaphenylbiphenyl is also a matter of interest. Nearly all computational methods find two distinct conformations for compound **1**. One of these possesses D_2 symmetry, and the other is the curiously distorted, C_1 -symmetric structure observed in the crystal. This is in agreement with a previous study, wherein extensive conformational searches using molecular mechanics could only find the D_2 and C_1 equilibrium conformations.² As summarized in Table 2, all three DFT methods employed here (and, indeed, every DFT method that we have ever applied to this problem) find the D_2 conformation (**1**) to be 13-20 $\text{kJ}\cdot\text{mol}^{-1}$ more stable than the C_1 conformation (**1a**). We assume, therefore, that decaphenylbiphenyl adopts the former conformation in the gas phase, but as shall be seen, the preference is less clear in the solid state.

Table 2. Computationally Estimated Relative Energies of D_2 (**1**) and C_1 (**1a**) Conformations of Decaphenylbiphenyl.



Level	ΔE ($\text{kJ}\cdot\text{mol}^{-1}$)	$\Delta(E+\text{ZPE})$ ($\text{kJ}\cdot\text{mol}^{-1}$)	ΔH_{298} ($\text{kJ}\cdot\text{mol}^{-1}$)
B3PW91/6-311G(d,p)	+13.0 ^a	+12.3 ^a	+13.0
M052X-D3/6-311G(d,p)	+19.0 ^a	+19.2 ^a	+19.8
PW6B95-D3(BJ)/6-311G(d,p)	+20.4 ^a	+19.8 ^a	+20.8
B3PW91/6-311++G(2d,p)	+11.7	+19.3	+19.8
M052X-D3/6-311++G(2d,p)	+17.1	+16.9	+17.6
PW6B95-D3(BJ)/6-311++G(2d,p)	+18.9	+18.7	+19.3

^a Ref. 3.

Synthesis and Characterization of Polyphenylbiphenyls. Decaphenylbiphenyl (**1**) was prepared on a multigram scale by a slight modification of the method of Ogliaruso and Becker,¹ and 2,2',4,4',6,6'-hexaphenylbiphenyl (**2**) was prepared as outlined by Fujioka et al.³⁷ Full details are provided in the Experimental section.

Compound **1** was initially purified by repeated crystallization from toluene. After drying under vacuum, the ¹³C NMR spectrum of this material still showed the presence of toluene. X-ray analysis of the crystals showed that it had crystallized as the toluene solvate (**1**•C₇H₈) in a structure that is nearly isomorphous with the triclinic literature chloroform solvate (**1**•CHCl₃). In both structures, the molecule of **1** possesses the higher-energy (as judged by DFT calculations) C₁ conformation. This conformation is easily recognized by the fact that one pair of phenyl groups *ortho* to the central bond lies face-to-face and the other pair is edge-to-face (see Figure 1). We speculated that the solvent molecule occupies a space in the structure that must be filled for the molecule of **1** to adopt the C₁ conformation. Perhaps crystallization from a larger solvent would yield a different, solvent-free crystal.

Crystallization from nitrobenzene gave a triclinic nitrobenzene solvate (**1**•C₆H₅NO₂) isomorphous with the previous structures (Figure 1). However, crystallization from 1,3,5-triisopropylbenzene gave a new, solvent-free, orthorhombic crystal form. In this structure, compound **1** adopts a conformation with approximate D₂ symmetry, recognizable by the two pairs of face-to-face phenyl groups *ortho* to the central bond (Figure 1).

Further drying and purification of compounds **1** and **2** was accomplished by repeated sublimation under reduced pressure. The sublimed sample of compound **1** yielded single crystals suitable for X-ray analysis. Most interestingly, these proved to be a new, solvent-free, triclinic crystal form which contains two crystallographically independent molecules of **1**, both adopting the C₁ conformation (Figure 2). It is this material that was used as the starting material for all thermochemical experiments.

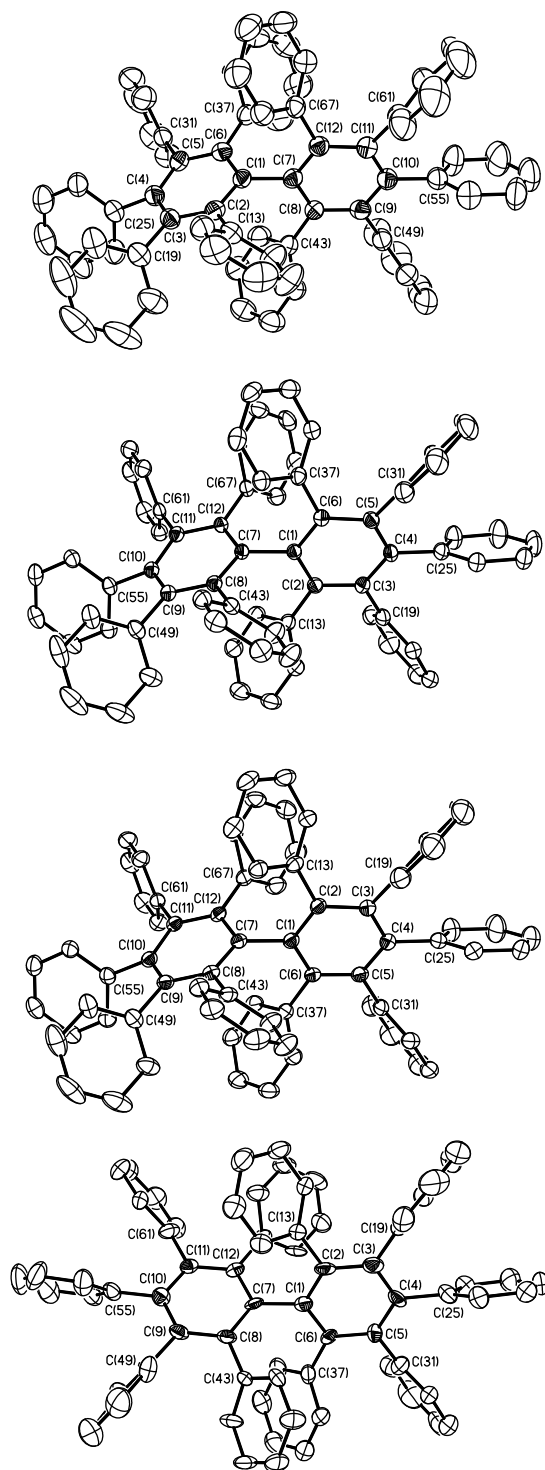


Figure 1. Molecular structures of decaphenylbiphenyl in (top to bottom) $1 \cdot \text{CHCl}_3$,² $1 \cdot \text{C}_7\text{H}_8$, $1 \cdot \text{C}_6\text{H}_5\text{NO}_2$, and **1** from triisopropylbenzene. Thermal ellipsoids have been drawn at the 50% probability level, and hydrogen atoms have been omitted for clarity.

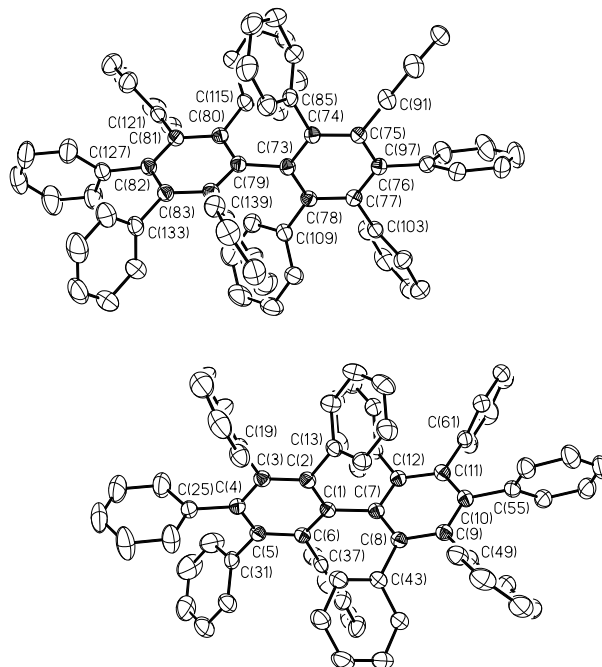


Figure 2. Molecular structures of two independent C_1 molecules in sublimed decaphenylbiphenyl, **1**. Thermal ellipsoids have been drawn at the 50% probability level, and hydrogen atoms have been omitted for clarity.

Evaluation of polymorphism in decaphenylbiphenyl by DSC. To elucidate the nature of the polymorphism of **1** we have performed DSC (differential scanning calorimetry) experiments of three different samples. Here we describe the DSC results of two consecutive cycles for each sample; each cycle consists of heating the sample from 30 °C to $T_m + 20$ °C (20 °C above the melting point), followed by cooling to 30 °C. A small hole was punctured on the top of the DSC crucibles to allow free release of evolving gases. Figure 3 shows the thermograms obtained for the first DSC heating runs of various samples. The results follow:

Sample I, toluene solvate ($I \cdot C_7H_8$, C_1 conformation). First, a large, broad endothermic peak with $T_{\text{onset}} = (137 \pm 1)$ °C is observed. This peak corresponds to the evaporation of toluene from the crystals, and integration of the DSC peak allowed us to estimate the enthalpy of toluene evaporation from **1** as $\Delta H_m = (45 \pm 5)$ kJ·mol⁻¹. After evaporation of toluene, a very small endothermic peak was observed at a variable temperature, $T_{\text{onset}} = [215, 290]$ °C, not reproducible from experiment to experiment. We tentatively attribute this peak to a crystal rearrangement

annealing after release of toluene. A third and last endothermic peak occurred at $T_{\text{onset}} = (331 \pm 1)^\circ\text{C}$ corresponding to the melting of **1**. Upon cooling, the compound crystallizes at an ill-defined temperature, $T_c \approx 180^\circ\text{C}$; the subsequent heating cycle reveals a very clean thermogram, with only the melting peak at $T_m = (331 \pm 1)^\circ\text{C}$ being observed.

Sample II, sublimed crystals of 1 (C_1 conformation). The first heating run is equivalent to the second cycle of Sample I, a clean thermogram showing only the melting peak at $T_m = (331 \pm 1)^\circ\text{C}$. On cooling, however, the liquid shows a significant tendency to undercool, and the glass was achieved in most of the experiments. In this case, the new heating run reveals the glass transition temperature, $T_g = (142 \pm 1)^\circ\text{C}$, followed by cold-crystallization at approximately 40°C above T_g (T_{cc} varies from 175°C to 200°C). After T_{cc} the crystal melts at the same temperature as before. The reason that Sample I crystallizes more easily on cooling is maybe due to the presence of some impurities that act as crystallization seeds. Bear in mind that Sample II was obtained from sublimation of Sample I under reduced pressure where a small brown non-volatile residue was observed during this purification process. Also of interest is one singular DSC run (the last cycle of an experiment with a total of five cycles) in which the melting peak was observed at a lower temperature than all the other runs. For this run, $T_m = 294^\circ\text{C}$, and this probably is due to the sporadic formation of a different polymorph.

Sample III, 1 from triisopropylbenzene (D_2 conformation). The DSC thermogram first reveals the endothermic loss of the crystallization solvent in a relatively large temperature range ($110 - 150^\circ\text{C}$). In contrast to Sample I, the solvent merely wets the crystals and is not part of a crystalline solvate. Following this process, the thermogram is clean, showing only a melting process occurring at $T_m = (290 \pm 1)^\circ\text{C}$ (lower than the other samples but similar to the sporadic result described for Sample II). After cooling the liquid, the new heating cycle shows T_g , T_{cc} , and melting, now at $T_m = (331 \pm 1)^\circ\text{C}$, as regularly observed for samples II. However, in one sporadic run of this sample (III.2 in Figure 3B) an exothermic peak was observed right after the melting of the D_2 polymorph, at $T_m = (290 \pm 1)^\circ\text{C}$. On further heating the sample, the melting at $T_m = (331 \pm 1)^\circ\text{C}$ occurred as previously observed for polymorph C_1 . In this way, the two

successive peaks represent the melting of polymorph D_2 followed by rapid crystallization into polymorph C_1 . From integration of the two peaks, we can estimate the enthalpy of the $D_2 \rightarrow C_1$ solid-solid phase transition as $\Delta H = 9 \text{ kJ}\cdot\text{mol}^{-1}$. This result should be regarded with care because there is no indication that these coupled peaks represent a true phase equilibrium and there is also no guarantee that all the melted liquid crystallized into the C_1 polymorph inside the crucible. To further explore this solid-solid phase transition we have made additional DSC experiments for dried Samples III. The samples were dried under vacuum at $T = 120 \text{ }^\circ\text{C}$ and $200 \text{ }^\circ\text{C}$. The DSC thermogram of the sample dried at $120 \text{ }^\circ\text{C}$ is shown in Figure 3A (III), and is similar to the original wetted sample, melting at $T_m = (290 \pm 1) \text{ }^\circ\text{C}$, but without loss of solvent. Interestingly, the DSC run of the sample dried at $200 \text{ }^\circ\text{C}$ shows a reproducible solid-solid phase transition at $T_{tr} = (218 \pm 2) \text{ }^\circ\text{C}$. However, after trying some cooling runs with changes to a variety of experimental parameters (cooling at different rates after the transition and holding isothermally at a lower temperature for some time) we never observed the reversible transition. After this phase transition the compound melts regularly at $T_m = (331 \pm 1) \text{ }^\circ\text{C}$. Based on our DSC and crystallographic results we attribute this peak to the $D_2 \rightarrow C_1$ solid-solid phase transition in **1**. The DSC results are shown in Figure 4. Our observations do not exclude the possibility that D_2 is metastable at lower temperatures, but the hypothesis that D_2 is thermodynamically more stable at low temperatures seems more likely (the chemical potentials of the two polymorphs shall cross at T_{tr}). The endothermic peak of this transition is highlighted in Figure 4A revealing a complex shape and an enthalpy of transition close to the sporadic run depicted in Figure 3B (III.2). Figure 4B elucidates the difference in the DSC baselines between the two polymorphs. This thermogram clearly indicates that polymorph D_2 has a larger $C_{p,m}^0$ than C_1 at temperatures lower than T_{tr} . This result was confirmed by the values of $C_{p,m}^0$, at $T = (298.15 \pm 0.02) \text{ K}$, measured by drop calorimetry in this work: $C_{p,m}^0(\mathbf{1}, C_1) = (1038.0 \pm 6.7)$ and $C_{p,m}^0(\mathbf{1}, D_2) = (1083.7 \pm 5.1) \text{ J}\cdot\text{K}^{-1}\cdot\text{mol}^{-1}$, indicating a quite significant difference between the polymorphs.

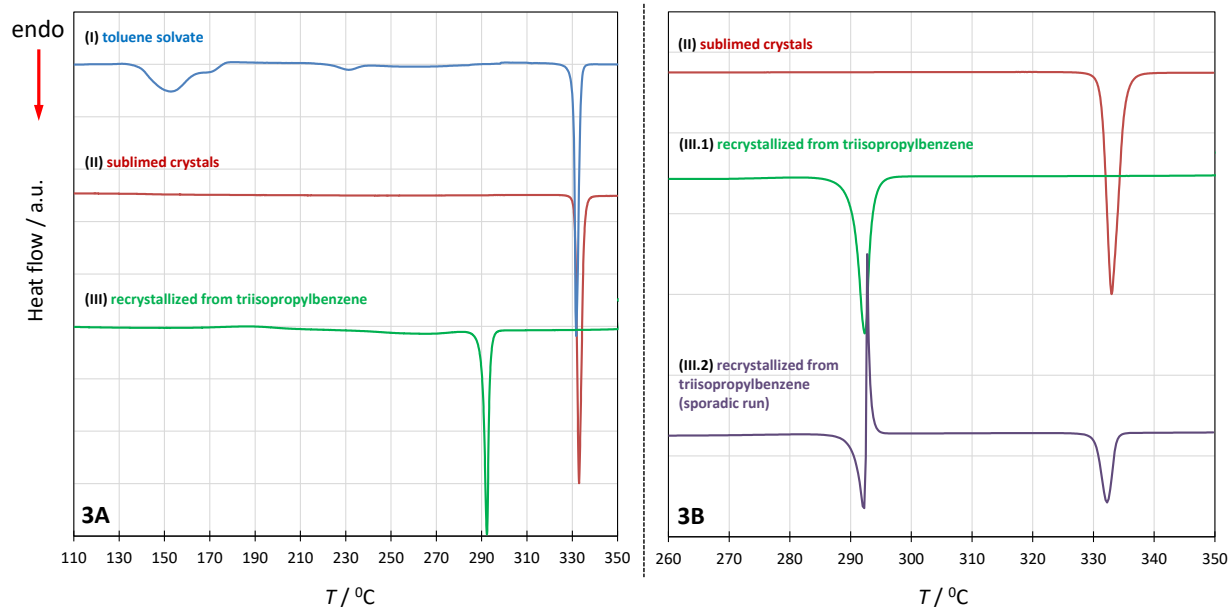


Figure 3. DSC thermograms (heating rate: $5 \text{ K} \cdot \text{min}^{-1}$) of various samples of compound **1**. 3A: (I) the toluene solvate ($\mathbf{1} \cdot \text{C}_7\text{H}_8$), (II) sublimed crystals of **1**, and (III) **1** from triisopropylbenzene dried under vacuum at $120 \text{ }^\circ\text{C}$. 3B: enlargement showing the melting of the two polymorphs: (II) sublimed crystals of **1**, (III.1) **1** from triisopropylbenzene, and (III.2) **1** from triisopropylbenzene (one sporadic run of sample III).

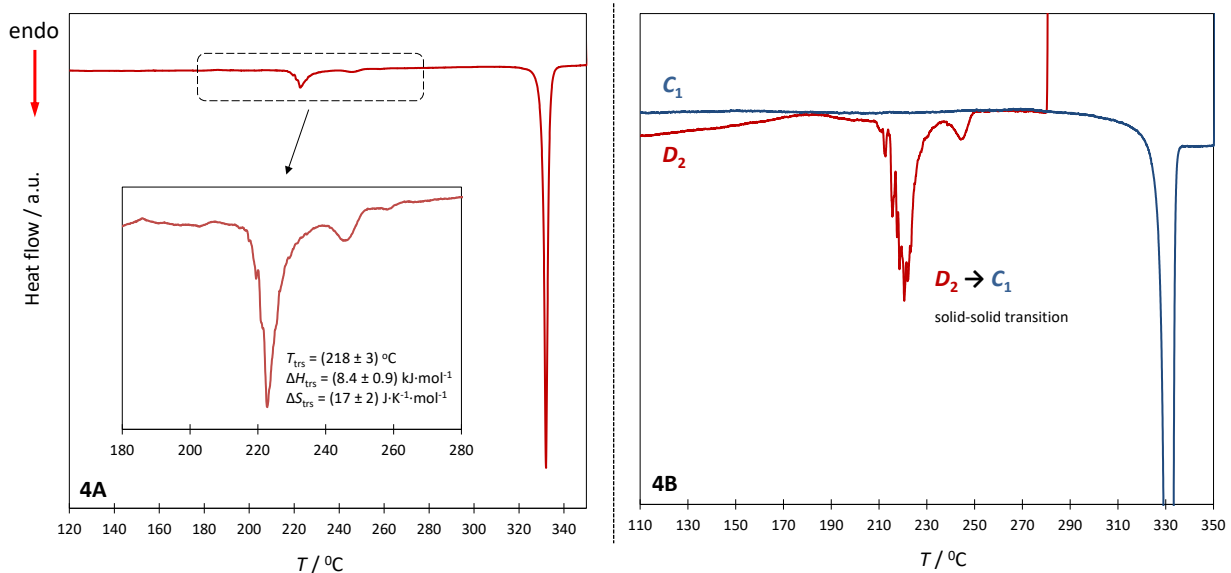


Figure 4. DSC thermograms of **1** recrystallized from triisopropylbenzene after drying under vacuum at $200 \text{ }^\circ\text{C}$. 4A: single heating run at $5 \text{ K} \cdot \text{min}^{-1}$ highlighting the observed endothermic solid-solid transition. 4B: heating run at $5 \text{ K} \cdot \text{min}^{-1}$ followed by cooling to $T = 100 \text{ }^\circ\text{C}$, after the solid-solid transition, and second heating cycle at $5 \text{ K} \cdot \text{min}^{-1}$ until melting of the C_1 polymorph.

These observations suggest that D_2 lies lower in energy than C_1 , which agrees with D_2 being the more stable molecular conformation. However, its larger $C_{p,m}^0$ increases $(\partial H/\partial T)_p$, a contribution that makes this polymorph less stable at higher temperatures. The reason why the C_1 polymorph has larger entropy is a matter of speculation; we propose that at mild to high temperatures the molecules can start interconverting dynamically between the two C_1 minima.

Apart from these data, no additional solid-solid transitions were observed in our DSC experiments. In conclusion, our results indicate the existence of two predominant polymorphic forms of the solvent-free crystals, the main difference between them being the molecular conformation. Polymorph C_1 has higher melting point and its greater stability at high temperatures is probably the result of its higher $S_m(\text{cr})$ relative to the D_2 polymorph. One cannot ignore the much greater tendency of **1** to crystallize as the C_1 polymorph. Precipitation from solvents and from the pure liquid, upon cooling and upon heating (T_{cc} after T_g), almost always yields this polymorph. The solid obtained by purifying **1** by sublimation is also the C_1 polymorph. However, the DSC results suggest that the D_2 polymorph is the more stable form at lower temperatures. It is lower in enthalpy than the C_1 polymorph, which may result from stronger intermolecular interactions and/or a more stable molecular conformation.

Although DFT calculations consistently find that the D_2 conformation is more stable in the gas phase, the preference in solution is unknown. Generally, continuum solvent models have little effect on the relative energies of hydrocarbon conformations and transition states.^{4,38} We have confirmed this by calculating the relative energies of the D_2 and C_1 conformations in benzene, using a polarizable continuum solvent model. The results are presented in the ESI† and clearly illustrate the small effect of including a continuum solvent model. Interconversion of the two conformations is very facile. At the B3PW91/6-31G(d) level of theory, where the D_2 conformation is $10.3 \text{ kJ}\cdot\text{mol}^{-1}$ lower in energy than the C_1 (very similar to the values found in Table 2), the transition state for the interconversion of the two conformers was located. For the C_1 to D_2 interconversion, the barrier is only $3.0 \text{ kJ}\cdot\text{mol}^{-1}$, and for the reverse reaction, the barrier is $13.3 \text{ kJ}\cdot\text{mol}^{-1}$. Such barriers are below the reach of low-temperature dynamic NMR

spectroscopy, and thus all NMR spectra of **1** are consistent with only *time-averaged* D_2 symmetry in solution. This molecular flexibility probably facilitates crystallization into the less stable C_1 polymorph.

Phase equilibria. From this point onwards, and according to the normal thermochemical practice, we use Kelvin (K) as the temperature unit. The thermodynamic properties associated with the melting process of compounds **1** and **2**, as evaluated by DSC, are presented in Table 3. As shown by Figures 3 and 4, compound **1** displays a rich phase behavior, which includes the observation of a glass transition and polymorphism. In contrast, compound **2** shows a simple DSC thermogram; melting is the only phase transition observed on heating and the corresponding crystallization occurs rapidly on cooling (approximately 60 K of undercooling). Heat capacity corrections were made to determine the enthalpies and entropies of melting at $\langle T \rangle$, where $\langle T \rangle$ is the average T_m of the samples being compared, and at $T = 298.15$ K (the detailed results and procedures are given in the ESI†). Herein, we assume $\Delta_{\text{cr}}^1 C_{\text{p,m}}^0 = +(54 \pm 20) \text{ J} \cdot \text{K}^{-1} \cdot \text{mol}^{-1}$, according to the equation proposed by Sidgwick³⁹ and recommended by Chickos.⁴⁰ We opt to make comparisons at $\langle T \rangle$ because it reduces substantially the extrapolation error associated with the heat capacity correction. It should, however, be kept in mind that comparisons are being made at a temperature significantly higher than 298.15 K. In Table 3 we present the DSC results for both polymorphs of compound **1**: C_1 from the samples of the sublimed crystals, and D_2 from the samples recrystallized from triisopropylbenzene, the wet samples and those dried at 120 °C give concordant results. For polymorph D_2 we chose to present only the values at T_m and $\langle T \rangle$ since the relatively large uncertainty in the values of $\Delta_{\text{cr}}^1 C_{\text{p,m}}^0$ make large extrapolations too speculative. Despite its smaller molar mass, compound **2** shows an enthalpically driven higher T_m . This suggests that in **1** the steric crowding is hampering the establishment of directional intermolecular contacts (e.g. C–H $\cdots\pi$ interactions), an effect that has more impact in the stability of the anisotropic crystal than of the isotropic liquid phase. This is a further indication that the maximization of intermolecular interactions is not the driving force for **1** to crystallize as the C_1 polymorph. Comparison between the two polymorphs

of **1** agrees qualitatively with the results for the solid-solid phase transition shown in Figure 4A, corroborating that, for low temperatures ($T < 220$ °C), the crystal of C_1 has greater enthalpy and entropy than the crystal D_2 ; note that the greater $C_{p,m}^0(\text{cr})$ of D_2 will make $\Delta_{\text{cr}}^1 H_m^0$ and $\Delta_{\text{cr}}^1 S_m^0$ larger relative to C_1 as T decreases. To better visualize phase stability and the thermodynamic differentiation between the two polymorphs of **1** we present in Figure 5 hypothetical enthalpy, entropy, and Gibbs energy diagrams showing their dependence with temperature for both C_1 , D_2 , and the liquid phase. These diagrams were built based on the following: (i) reported values of phase transitions (figure 4A and table 3); (ii) reported values of $C_{p,m}^0(\text{cr})$ for both polymorphs; (iii) assuming $C_{p,m}^0(\text{l}) > C_{p,m}^0(\text{cr})$; (iv) assuming $C_{p,m}^0$ independent of T in the temperature interval considered; and (v) assuming that the $D_2 \rightarrow C_1$ transition is a thermodynamic reversible phase transition occurring at $T = 218$ °C = 491 K.

Table 3. Melting (T_m), glass transition temperatures (T_g), and derived standard molar enthalpies ($\Delta_{\text{cr}}^1 H_m^0$), and entropies ($\Delta_{\text{cr}}^1 S_m^0$) of melting for compounds **1** and **2**, at T_m , $\langle T \rangle = (600.5 \pm 0.1)$ K, where $\langle T \rangle$ is the average T_m of the three samples, and $T = 298.15$ K.

	T / K	$\Delta_{\text{cr}}^1 H_m^0 / \text{kJ} \cdot \text{mol}^{-1}$	$\Delta_{\text{cr}}^1 S_m^0 / \text{J} \cdot \text{K}^{-1} \cdot \text{mol}^{-1}$
Decaphenylbiphenyl (1 , D_2)	$T_m = 563.3 \pm 0.1$	$55.4 \pm 2.0 (T_m)$	$98.3 \pm 3.5 (T_m)$
		$57.4 \pm 2.1 (\langle T \rangle)$	$101.8 \pm 3.7 (\langle T \rangle)$
Decaphenylbiphenyl (1 , C_1)	$T_m = 603.8 \pm 0.1$	$59.1 \pm 2.5 (T_m)$	$97.9 \pm 4.1 (T_m)$
	$T_g = 415.1 \pm 0.2$	$58.9 \pm 2.5 (\langle T \rangle)$	$97.6 \pm 4.1 (\langle T \rangle)$
	$(T_g/T_m = 0.69)$	$42.5 \pm 6.6 (298.15 \text{ K})$	$60 \pm 15 (298.15 \text{ K})$
Hexaphenylbiphenyl (2)	$T_m = 634.4 \pm 0.1$	$71.8 \pm 2.7 (T_m)$	$113.2 \pm 4.2 (T_m)$
		$70.0 \pm 2.8 (\langle T \rangle)$	$110.2 \pm 4.3 (\langle T \rangle)$
		$53.5 \pm 7.2 (298.15 \text{ K})$	$72 \pm 16 (298.15 \text{ K})$

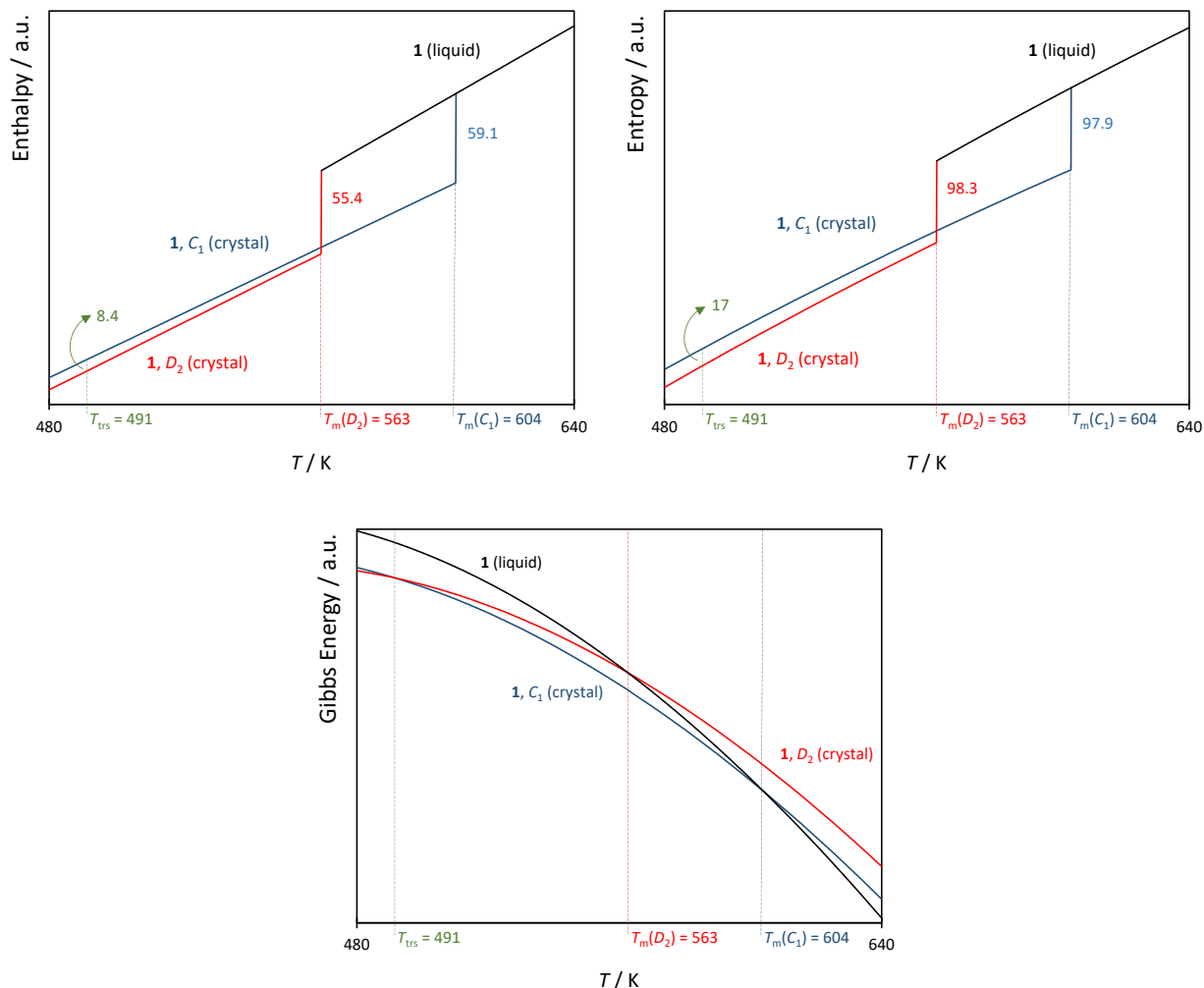


Figure 5. Hypothetical enthalpy (left), entropy (right), and Gibbs energy (bottom) diagrams for the C_1 (blue) and D_2 (red) polymorphs of decaphenylbiphenyl, **1**, and its liquid phase, as a function of temperature. Values of standard molar enthalpies of phase transitions in $\text{kJ}\cdot\text{mol}^{-1}$ and entropies in $\text{J}\cdot\text{K}^{-1}\cdot\text{mol}^{-1}$.

The solid-gas equilibrium was evaluated by measuring the vapor pressures (0.1 to 1.0 Pa) of the compounds studied in a temperature range of about 20 K using the Knudsen effusion methodology. For the heat capacity corrections of the thermodynamic parameters from the average $\langle T \rangle$ of the sublimation experiments to $T = 298.15$ K, we have calculated the values of $\Delta_{\text{cr}}^{\text{g}} C_{p,m}^0 = C_{p,m}^0(\text{g}) - C_{p,m}^0(\text{cr})$ for **1** and **2** using the values of $C_{p,m}^0(\text{g})$ calculated at the M052X-D3/6-311++G(2d,p) level of theory and the values of $C_{p,m}^0(\text{cr})$ measured by drop calorimetry in this work. For 1,2,3,5-tetraphenylbenzene (**7**), and due to the significantly smaller temperature

extrapolation required in the heat capacity correction, we have assumed $\Delta_{\text{cr}}^{\text{g}}C_{p,m}^0 = -(35 \pm 8) \text{ J}\cdot\text{K}^{-1}\cdot\text{mol}^{-1}$, which is a typical value for polyphenylbenzenes and similar organic compounds.^{31,41}

The heat capacity data is shown in Table 4. The detailed sublimation results and procedures for the determination of the thermodynamic functions of sublimation ($\Delta_{\text{cr}}^{\text{g}}H_{\text{m}}^0$, $\Delta_{\text{cr}}^{\text{g}}S_{\text{m}}^0$ and $\Delta_{\text{cr}}^{\text{g}}G_{\text{m}}^0$) are presented in the ESI†.

Table 4. Heat capacity values, at $T = 298.15 \text{ K}$, for compounds **1**, **2**, and **7**; the values of $C_{p,m}^0(\text{g})$ were calculated at the M052X-D3/6-311++G(2d,p) level (using the reported frequency scale factor of 0.962⁴²) and those of $C_{p,m}^0(\text{cr})$ were measured by Drop Calorimetry.

	$C_{p,m}^0(\text{g}) / \text{J}\cdot\text{K}^{-1}\cdot\text{mol}^{-1}$	$C_{p,m}^0(\text{cr}) / \text{J}\cdot\text{K}^{-1}\cdot\text{mol}^{-1}$	$\Delta_{\text{cr}}^{\text{g}}C_{p,m}^0{}^a / \text{J}\cdot\text{K}^{-1}\cdot\text{mol}^{-1}$
Decaphenylbiphenyl (1 , C_{10})	991.0	1038.0 ± 6.7	-47 ± 8
Hexaphenylbiphenyl (2)	658.6	689.4 ± 4.1	-31 ± 8
1,2,3,5-Tetraphenylbenzene (7)	n.a.	n.a.	$-35 \pm 8{}^b$

^a The uncertainty in $\Delta_{\text{cr}}^{\text{g}}C_{p,m}^0$ was taken as $\pm 8 \text{ J}\cdot\text{K}^{-1}\cdot\text{mol}^{-1}$ in all cases to include unaccounted uncertainty in the theoretical values of $C_{p,m}^0(\text{g})$. ^b Estimated value.^{31,41}

Table 5 lists the derived standard ($p^0 = 10^5 \text{ Pa}$) molar enthalpies, entropies, and Gibbs energies of sublimation, at $T = 298.15 \text{ K}$, for compounds **1**, **2**, and **7**. For comparison we also show in this table the literature values for other similar polyphenylbenzenes. The results presented in Table 5 reveal the relatively low $\Delta_{\text{cr}}^{\text{g}}H_{\text{m}}^0$ and $\Delta_{\text{cr}}^{\text{g}}S_{\text{m}}^0$ of **1** and **2**, despite their quite large molecular size. This is easily understood by considering the accessible surface area of the molecules. The crowding of phenyl groups reduces intermolecular contacts and the vibrational and rotational freedom of each phenyl ring. This situation is particularly dire in compound **1**, wherein a very substantial part of the molecule is precluded from establishing intermolecular contacts. Moreover, the internal rotation of all phenyl rings is severely hampered by adjacent groups, contributing to a lower entropic gain upon sublimation. To examine the sublimation data in more detail, we have calculated, for each polyphenylbenzene, the fraction of intermolecular interaction enthalpy per phenyl ring relative to benzene, $f_{\Delta H}$, using Eq. 4, and the average contribution per phenyl ring to $\Delta_{\text{cr}}^{\text{g}}H_{\text{m}}^0$, $\Delta H(\text{Ph})$, using Eq. 5:

$$f_{\Delta H} = \Delta_{\text{cr}}^{\text{g}}H_{\text{m}}^0(\text{compound}) / (\Delta_{\text{cr}}^{\text{g}}H_{\text{m}}^0(\text{benzene}) \cdot n(\text{Ph})) \quad (\text{Eq. 4})$$

$$\Delta H(\text{Ph}) = \Delta_{\text{cr}}^{\text{g}}H_{\text{m}}^0 / n(\text{Ph}) \quad (\text{Eq. 5})$$

where $n(\text{Ph})$ is the total number of phenyl rings in the compound. In this comparative analysis we include all the relevant polyphenylbenzenes reported in the literature and benzene is considered the reference. The results are shown in Table 6, which reveals some clear trends. As expected, the strength of intermolecular interactions increases in the order *ortho* < *meta* < *para*-series. Except for the *para*-series, $f_{\Delta H}$ decreases with $n(\text{Ph})$, and this decrease is more marked in the *ortho*-series. Compound **1** has clearly the lowest value of $\Delta H(\text{Ph})$, followed by the also crowded hexaphenylbenzene and **2**. Figure 6 plots $\Delta H(\text{Ph})$ as a function of $n(\text{Ph})$ for four series of polyphenylbenzenes: *ortho*-, *meta*-, and *para*-polyphenylbenzenes, and substituted biphenyls (biphenyl, **7**, **2**, and **1**); all series start with biphenyl. The decrease in $\Delta H(\text{Ph})$ is quite substantial in the *ortho*- and biphenyl-series. The results nicely follow the decrease in the relative surface area of the molecules (fraction available for intermolecular interactions) as more phenyl rings cluster near each other and go in line with the previous findings of Lima et al.^{31,41} and Wuest and co-workers.⁴³

Table 5. Standard ($p^0 = 10^5$ Pa) molar enthalpies, entropies, and Gibbs energies of sublimation, at $T = 298.15$ K, for the compounds studied and similar compounds reported in the literature.

	$\Delta_{\text{cr}}^{\text{g}}H_{\text{m}}^0 / \text{kJ}\cdot\text{mol}^{-1}$	$\Delta_{\text{cr}}^{\text{g}}S_{\text{m}}^0 / \text{J}\cdot\text{K}^{-1}\cdot\text{mol}^{-1}$	$\Delta_{\text{cr}}^{\text{g}}G_{\text{m}}^0 / \text{kJ}\cdot\text{mol}^{-1}$
Decaphenylbiphenyl (1 , C_{10})	216.3 ± 2.1	295.5 ± 5.0	128.2 ± 2.6
Hexaphenylbiphenyl (2)	204.7 ± 1.9	281.7 ± 4.7	120.7 ± 2.4
1,2,3,5-Tetraphenylbenzene (7)	162.9 ± 1.2	266.0 ± 3.2	83.5 ± 1.5
Biphenyl ³⁴	81.5 ± 0.2	180.3 ± 0.5	27.7 ± 0.2
1,3,5-Triphenylbenzene ³⁵	147.8 ± 0.7	254.0 ± 2.0	72.1 ± 0.9
Pentaphenylbenzene ³¹	170.2 ± 1.3	268.6 ± 3.4	90.1 ± 1.6
Hexaphenylbenzene ⁴¹	175.5 ± 2.1	245.4 ± 5.2	102.3 ± 2.6

Table 6. Standard ($p^0 = 10^5$ Pa) molar enthalpies of sublimation, at $T = 298.15$ K, for several phenylbenzene derivatives and their comparative analysis relative to benzene.

	$n(\text{Ph})$	$\Delta_{\text{cr}}^{\text{g}} H_{\text{m}}^0 /$ $\text{kJ}\cdot\text{mol}^{-1}$	$f_{\Delta H}^a$	$\Delta H(\text{Ph})^b /$ $\text{kJ}\cdot\text{mol}^{-1}$
<i>para</i> -series				
Benzene ³²	1	44.7 ± 0.2^c	1.00	44.7 ± 0.2
Biphenyl ³⁴	2	81.5 ± 0.2	0.91	40.8 ± 0.1
<i>p</i> -Terphenyl ⁴⁴	3	125.6 ± 0.8	0.94	41.9 ± 0.3
<i>p</i> -Quaterphenyl ³²	4	168.4 ± 1.6	0.94	42.1 ± 0.4
<i>meta</i> -series				
Biphenyl ³⁴	2	81.5 ± 0.2	0.91	40.8 ± 0.1
<i>m</i> -Terphenyl ⁴⁴	3	118.6 ± 0.7	0.88	39.5 ± 0.2
1,3,5-Triphenylbenzene ³⁵	4	147.8 ± 0.7	0.83	37.0 ± 0.2
<i>ortho</i> -series				
Biphenyl ³⁴	2	81.5 ± 0.2	0.91	40.8 ± 0.1
<i>o</i> -Terphenyl ⁴⁴	3	103.0 ± 0.4	0.77	34.3 ± 0.1
1,2,3-Triphenylbenzene ³⁵	4	134.1 ± 1.1	0.75	33.5 ± 0.3
1,2,3,4-Tetraphenylbenzene ³¹	5	154.1 ± 1.9	0.69	30.8 ± 0.4
Pentaphenylbenzene ³¹	6	170.2 ± 1.3	0.63	28.4 ± 0.2
Hexaphenylbenzene ⁴¹	7	175.5 ± 2.1	0.56	25.1 ± 0.3
Decaphenylbiphenyl (1 , C_1)	12	216.3 ± 2.1	0.40	18.0 ± 0.2
1,2,3,5-Tetraphenylbenzene (7)	5	162.9 ± 1.2	0.73	32.6 ± 0.3
Hexaphenylbiphenyl (2)	8	204.7 ± 1.9	0.57	25.6 ± 0.2

^a Fraction of intermolecular interaction enthalpy per phenyl ring relative to benzene. ^b Average contribution of each phenyl ring to $\Delta_{\text{cr}}^{\text{g}} H_{\text{m}}^0$, at $T = 298.15$ K. ^c Derived hypothetical value refer to conditions of temperature and pressure at which benzene is a liquid; see Ref. 32 for details.

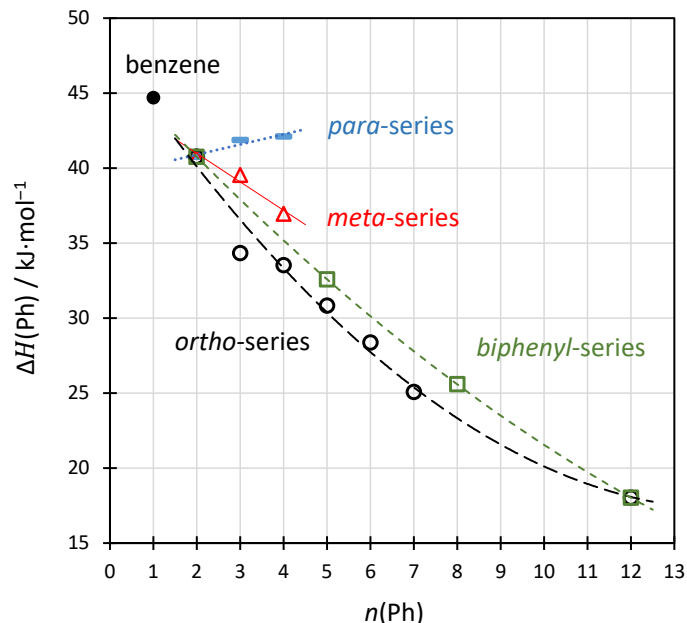


Figure 6. Graphical representation of $\Delta H(\text{Ph})$, at $T = 298.15 \text{ K}$, as a function of the total number of phenyl rings, $n(\text{Ph})$, in various series of polyphenylbenzenes; all series start with biphenyl and **1** is included in the *ortho*- and biphenyl-series correlations.

If comparing the biphenyls **1** and **2** to their benzene analogues, hexaphenylbenzene and **7**, respectively, it is interesting to note that (i) the biphenyls have lower $\Delta H(\text{Ph})$ than the corresponding benzenes and (ii) **2** and hexaphenylbenzene have similar $\Delta H(\text{Ph})$ despite the less crowded molecular structure of **2**. Inspection of the corresponding X-ray structures reveals that, while the central benzene ring of hexaphenylbenzene⁴¹ and **7**⁴⁵ participate in well-defined intermolecular C–H $\cdots\pi$ interactions, the two central rings of **1** do not establish clear stabilizing contacts with neighboring molecules, and only one of the central rings of **2** has (two) such contacts. Hence, the results indicate that the central rings of **1** and **2** have a very weak contribution to the cohesive energy of the solid phase. In the case of **1**, one cannot forget that D_2 is probably the most stable conformation in the gas phase. In that case, the sublimation process of **1** includes an exothermic conformational change, which also contributes to decrease $\Delta_{\text{cr}}^{\text{g}} H_{\text{m}}^0$. Together, the results for phase equilibria illustrate the weakening of intermolecular interactions due to steric crowding in heavily substituted phenylbenzene derivatives. The clustering of rings around a central aromatic unit progressively precludes more π -faces from participating in

substantial intermolecular contacts, such as C–H $\cdots\pi$ and $\pi\cdots\pi$ interactions. This clustering of rings also imposes significant steric restraints to Ph-Ph torsion, which decreases $S_m(l)$ and $S_m(g)$, and consequently $\Delta_{cr}^1 S_m^0$ and $\Delta_{cr}^g S_m^0$.

Aiming for a more comprehensive analysis of the phase equilibria of **1** and **2**, the standard molar enthalpies, and entropies of vaporization, at $T = 298.15$ K, were estimated as:

$$\Delta_1^g X_m^0 = \Delta_{cr}^g X_m^0 - \Delta_{cr}^1 X_m^0 \quad (\text{Eq. 6})$$

where $X = H, S$, and using the values presented in tables 3 and 5. The standard molar Gibbs energies of vaporization were calculated as $\Delta_1^g G_m^0 = \Delta_1^g H_m^0 - T \cdot \Delta_1^g S_m^0$, for $T = 298.15$ K. The results are presented in Table 7. Note that the increase in ΔG , ΔH , and ΔS from **2** to **1** is more significant in the vaporization process than in sublimation. As can also be perceived from the melting results (e.g., **1** has lower T_m but greater $\Delta_{cr}^g G_m^0$ than **2**), the destabilizing effects in **1** are manifested to their greatest extent in the crystal phase. Remember that **1** probably adopts its most stable D_2 conformation in liquid and gas phases, which also contributes to the relative destabilization of the C_1 crystal. However, our results have shown that the C_1 polymorph has the highest T_m , being the most stable at high temperatures. Therefore, the lower ability, due to steric crowding, of **1** to participate in intermolecular contacts with orientational requisites (C–H $\cdots\pi$ and $\pi\cdots\pi$ interactions) is also negatively affecting the crystal more than it affects the liquid. This makes sense considering that in the liquid the contribution of such orientational interactions is diluted due to molecular motions. Consequently, the intermolecular potential has a greater contribution from purely dispersive interactions, which are more dependent on molecular size.

Table 7. Standard molar enthalpies, entropies, and Gibbs energies of vaporization, at $T = 298.15$ K, for the compounds studied.

	$\Delta_1^g H_m^0 / \text{kJ}\cdot\text{mol}^{-1}$	$\Delta_1^g S_m^0 / \text{J}\cdot\text{K}^{-1}\cdot\text{mol}^{-1}$	$\Delta_1^g G_m^0 / \text{kJ}\cdot\text{mol}^{-1}$
Decaphenylbiphenyl (1)	174 ± 7	236 ± 16	104 ± 8
Hexaphenylbiphenyl (2)	151 ± 7	210 ± 16	89 ± 9

Gas phase molecular energetics. Following our initial computational analysis, we now present the experimental evaluation of molecular energetics in the crowded biphenyls studied. The energetics of solids **1**, **2**, and **7** were quantified by high precision combustion calorimetry. Table 8 lists the derived standard molar enthalpies of combustion, $\Delta_c H_m^0(\text{cr})$, and the standard molar enthalpies of formation, $\Delta_f H_m^0$, in the crystalline and gaseous phases, at $T = 298.15$ K. To derive $\Delta_f H_m^0(\text{cr})$ from $\Delta_c H_m^0(\text{cr})$, the standard molar enthalpies of formation of $\text{H}_2\text{O}(\text{l})$ and $\text{CO}_2(\text{g})$ at $T = 298.15$ K, $-(285.830 \pm 0.042)$ and $-(393.51 \pm 0.13)$ $\text{kJ}\cdot\text{mol}^{-1}$, respectively, were used.⁴⁶ In accordance with normal thermochemical practice, the combined expanded uncertainty assigned to $\Delta_c H_m^0(\text{cr})$ is twice the overall standard deviation of the mean and includes the uncertainties in calibration and in the auxiliary quantities used; the uncertainty in $\Delta_f H_m^0(\text{cr})$ is the combined standard uncertainty. The detailed results are presented as ESI†.

Table 8. Standard ($p^0 = 10^5$ Pa) molar enthalpies of combustion, $\Delta_c H_m^0(\text{cr})$, and standard molar enthalpies of formation in the crystalline state, $\Delta_f H_m^0(\text{cr})$, and in the gas phase, $\Delta_f H_m^0(\text{g})$, at $T = 298.15$ K, for the compounds studied.

	$\Delta_c H_m^0(\text{cr}) / \text{kJ}\cdot\text{mol}^{-1}$	$\Delta_f H_m^0(\text{cr}) / \text{kJ}\cdot\text{mol}^{-1}$	$\Delta_f H_m^0(\text{g}) / \text{kJ}\cdot\text{mol}^{-1}$
Decaphenylbiphenyl (1) ^a	-36445.9 ± 11.3	967.4 ± 14.7	1183.7 ± 14.8
Hexaphenylbiphenyl (2)	-24301.0 ± 7.8	553.4 ± 10.0	758.1 ± 10.2
1,2,3,5-Tetraphenylbenzene (7)	-15272.4 ± 5.3	322.9 ± 6.6	485.8 ± 6.7

^a Crystal phase refers to the C_1 polymorph.

For the evaluation of gas-phase energetics, the standard molar enthalpies of formation in the gas phase, $\Delta_f H_m^0(\text{g})$, at $T = 298.15$ K, for compounds **1**, **2**, and **7** were calculated as:

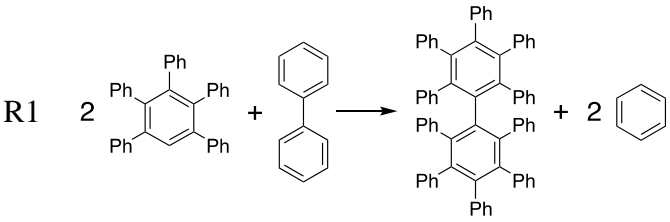
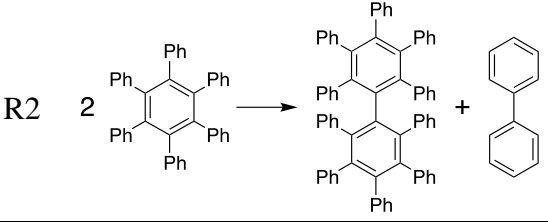
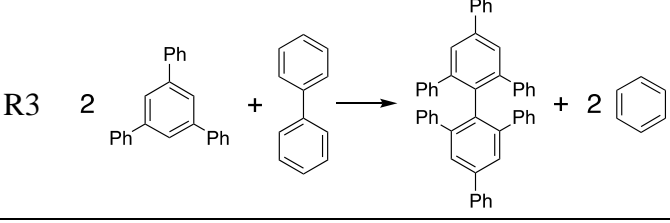
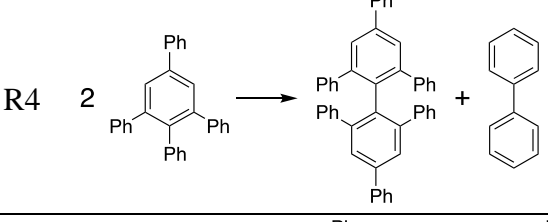
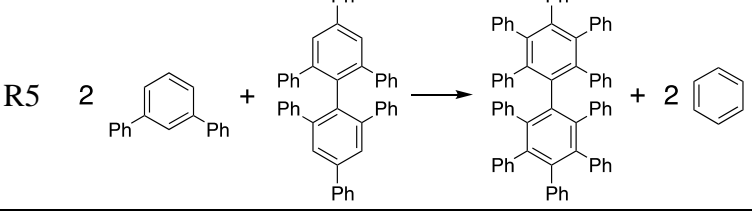
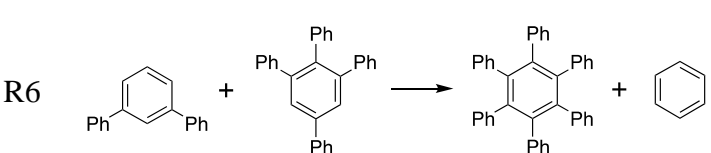
$$\Delta_f H_m^0(\text{g}, 298.15 \text{ K}) = \Delta_f H_m^0(\text{cr}, 298.15 \text{ K}) + \Delta_{\text{cr}}^{\text{g}} H_m^0(298.15 \text{ K}) \quad (\text{Eq. 7})$$

Due to the polymorphism of compound **1**, and in order to apply Eq. 7 correctly, we had to make sure that $\Delta_f H_m^0$ and $\Delta_{\text{cr}}^{\text{g}} H_m^0$ were measured for the same solid phase. To this end we employed the following procedures: (i) we used the same sublimed sample of **1** for the Knudsen and combustion experiments; (ii) we verified by DSC, before and after the combustion and sublimation studies, that the samples were of the C_1 polymorph and that no phase transition occurs between room temperature and the melting point; and (iii) we performed an additional set of combustion experiments with the remaining sample from the Knudsen measurements (showing concordant results with the original sample). Therefore, all Knudsen and combustion results refer to the C_1 polymorph of compound **1**.

In Table 9 we present the experimental standard molar enthalpies of reaction in the gas phase, $\Delta_{\text{react}} H_m^0(\text{g})$, at $T = 298.15 \text{ K}$, for some selected homodesmotic reactions. The values of $\Delta_f H_m^0(\text{cr})$ for all the compounds presented in these reaction schemes were determined by combustion calorimetry. In this way, in the calculation of the uncertainties in $\Delta_{\text{react}} H_m^0(\text{g})$ for all the homodesmotic reactions, some contributions cancel out and can be ignored in this comparative analysis: (i) uncertainties related to the formation of $\text{CO}_2(\text{g})$ and $\text{H}_2\text{O}(\text{l})$ in the corresponding combustion reactions cancel out completely, and (ii) uncertainties related to the calibration of the calorimeters cancel out to a great extent (depending on the type of calorimeter and calibrant used). In Table 9 the computational results for the homodesmotic reactions using PW6B95-D3(BJ)/6-311++G(2d,p) and M052X-D3/6-311++G(2d,p) are listed for comparison. Remember that the experimental and calculated enthalpies of reaction can be compared directly because both refer to the same states of the ideal gases at $T = 298.15 \text{ K}$.

The UV results presented in the ESI† support the absence of any meaningful inter-ring π -conjugation in **1** and **2**, as it would be expected for aromatic compounds with large Ph-Ph dihedral angles. It is therefore safe to neglect the contribution of conjugation for the energetics of these molecules.

Table 9. Experimental and calculated (PW6B95-D3(BJ)/6-311++G(2d,p) and [M052X-D3/6-311++G(2d,p)]) standard ($p^0 = 10^5$ Pa) molar enthalpies of reaction in the gas phase, $\Delta_{\text{react}}H_{\text{m}}^0(\text{g})$, at $T = 298.15$ K, for selected homodesmotic reaction schemes.^a

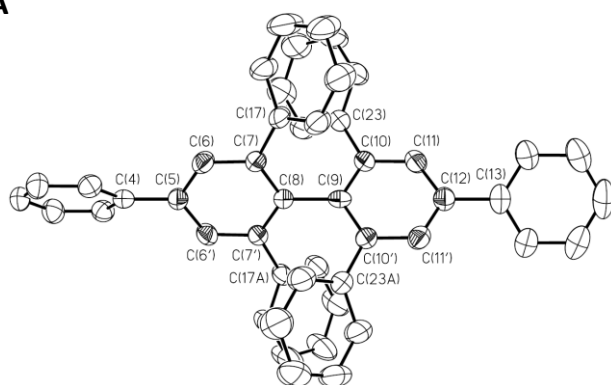
Homodesmotic reaction	$\Delta_{\text{react}}H_{\text{m}}^0(\text{g}) / \text{kJ}\cdot\text{mol}^{-1}$		
	ΔH_{exptl}	$\Delta H_{\text{calcd}}^b$	$\Delta\Delta H^b$
	-25 ± 10	-5 [+2]	+20 [+27]
	-25 ± 8	-27 [-16]	-2 [+9]
	8 ± 7	-12 [-6]	-20 [-14]
	-31 ± 8	-34 [-26]	-3 [+5]
	32 ± 10	+54 [+49]	+25 [+17]
	13 ± 6	+23 [+19]	+10 [+6]

^a The following literature values of $\Delta_f H_{\text{m}}^0(\text{g})$, in $\text{kJ}\cdot\text{mol}^{-1}$, were used for the calculation of the tabulated $\Delta_{\text{react}}H_{\text{m}}^0(\text{g})$: benzene (82.9 ± 0.9),^{32,47} biphenyl (182.0 ± 0.7),³⁴ *m*-terphenyl (279.9 ± 3.9),⁴⁴ 1,3,5-triphenylbenzene (366.8 ± 4.9),³⁵ pentaphenylbenzene (596.5 ± 9.1),³¹ and hexaphenylbenzene (695.6 ± 8.3).⁴¹ ^b For each entry the PW6B95-D3(BJ) result is first and the M052X-D3 is below it, in square brackets.

The significant exothermicity of R1 reveals a very significant stabilization of **1** if the crowding of phenyls around a central benzene ring is considered (by using pentaphenylbenzene in the homodesmotic reaction). A similar stabilization of **1** is observed when using hexaphenylbenzene instead of pentaphenylbenzene in the homodesmotic scheme (R2 in Table 9). This is in accordance with a previous work showing that the destabilization of penta- and hexaphenylbenzene, due to steric crowding, is (18 ± 7) $\text{kJ}\cdot\text{mol}^{-1}$ in both molecules.³¹ Hence, the contribution of steric crowding in **1** is effectively canceled out in these two homodesmotic reactions. The reason why $\Delta_{\text{react}}H_{\text{m}}^0(\text{g})$ for R1 and R2 is exothermic is probably the existence of stabilizing intramolecular interactions between the substituents of each central ring in **1**. The typical aromatic interaction between two benzene rings is about $12 \text{ kJ}\cdot\text{mol}^{-1}$ (both for parallel-displaced and T-shaped interacting rings).⁴⁸⁻⁵³ The magnitude of $\Delta_{\text{react}}H_{\text{m}}^0(\text{g})$ for R1 is consistent with the existence of two aromatic interactions in **1**. In fact, the X-ray crystal structures of **1** show the existence of various intramolecular contacts within typical aromatic interaction distances.⁴⁹⁻⁵¹ While in the C_1 polymorph these interactions can involve the *ortho* and *meta* rings in both sides of the molecule, in the D_2 polymorph the *ortho*-rings establish the most meaningful intramolecular contacts. Without being certain which conformation of **1** is the most stable in the gas phase, we can conclude that the spatial clustering of the rings in the molecule of **1** yields a global stabilization of (25 ± 8) $\text{kJ}\cdot\text{mol}^{-1}$ due mostly to intramolecular London dispersion. The homodesmotic reactions R3 and R4 in Table 9 show the analogous results for compound **2**. In the case of R3 we cannot assume that attractive forces in **2** are the only significant contribution to $\Delta_{\text{react}}H_{\text{m}}^0(\text{g})$, because the steric crowding between three adjacent phenyl rings in **2** is not canceled out in 1,3,5-triphenylbenzene. In fact, R3 allows us to see that there is still some destabilization in **2** due to steric crowding. The existence of such steric repulsion is nicely evidenced by comparing the values of $\Delta_{\text{f}}H_{\text{m}}^0(\text{g})$ between the isomers 1,3,5-triphenylbenzene (366.8 ± 4.9) $\text{kJ}\cdot\text{mol}^{-1}$, and 1,2,3-triphenylbenzene (376.7 ± 5.3) $\text{kJ}\cdot\text{mol}^{-1}$.³⁵ Alternatively, we use R4 to better evaluate the magnitude of dispersive interactions in the molecule of **2**. The use of 1,2,3,5-tetraphenylbenzene (**7**) in the homodesmotic scheme

effectively cancels the contributions from steric crowding and ring position, evidencing a significant stabilization of $(31 \pm 8) \text{ kJ}\cdot\text{mol}^{-1}$ in **2**. The X-ray structure of **2** reveals two aromatic parallel-displaced interactions (between the *ortho*-rings of each central benzene) at near-optimal centroid-centroid distance of 4.06 \AA^{49-51} (see Figure 7), suggesting that a large fraction of this stabilization comes from these intramolecular contacts. These results constitute experimental evidence that crowded biphenyls can be substantially stabilized by intramolecular dispersion.

7A



7B

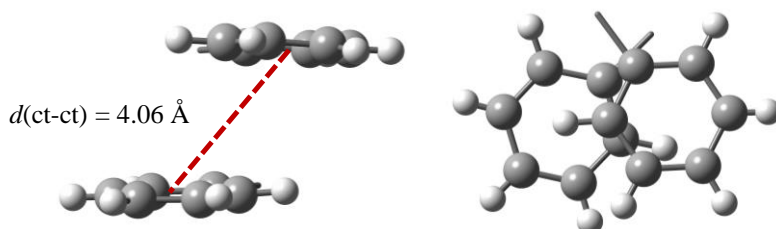


Figure 7. (A) Molecular structure of **2** in the crystal phase emphasizing the geometry of the four interacting *ortho*-rings; and (B) side and top views of the interacting pair, $d(\text{ct-ct})$ is the centroid-centroid distance between the interacting rings (the rest of the molecule was omitted for clarity).

The homodesmotic reaction R5 compares compounds **1** and **2** directly. The large endothermic $\Delta_{\text{react}}H_{\text{m}}^0(\text{g})$ for R5 clearly reveals that **1**, like penta- and hexaphenylbenzene, still suffers from significant steric repulsions. If comparing R5 and R6 in Table 9 one can see that $\Delta_{\text{react}}H_{\text{m}}^0(\text{g}, \text{R5}) \approx 2 \cdot \Delta_{\text{react}}H_{\text{m}}^0(\text{g}, \text{R6})$, corroborating that the energetic penalty due to steric

crowding in each central ring of **1** is comparable to hexaphenylbenzene. Additionally, this consistency in energetic data is a strong sign that molecules **1** and **2** share the same origin of intramolecular stabilization. The $\sim 30 \text{ kJ}\cdot\text{mol}^{-1}$ of stabilization in both molecules is probably arising from two intramolecular parallel-displaced aromatic interactions involving the four *ortho*-rings. In this context, the *meta*-rings in **1** are just introducing steric repulsions, analogously to what happens in hexaphenylbenzene, and shall not contribute significantly to increase intramolecular dispersion forces. This makes sense if considering that the D_2 conformer of **1**, in which the *meta*-rings do not participate in significant stabilizing contacts, is the most stable in the gas phase, which, according to our computational calculations, is probably the case.

As shown in Table 1, the DFT calculations for **1** significantly underestimate its stabilization. The exaggerated destabilization predicted by B3PW91, which cannot describe London dispersion, is partially corrected by using the dispersion-corrected functionals M052X-D3 and PW6B95-D3(BJ). Notwithstanding, the failing of uncorrected functionals to reproduce the energetics of these molecules support the conclusion that a large fraction of the stabilization in **1** and **2** comes from intramolecular dispersive interactions. Concerning the results in Table 9, experiment and theory show very nice agreement for R2 and R4, which are in fact the most well-balanced homodesmotic reactions. Interestingly, the calculations fail in all those cases where the steric constraint around benzene is not balanced in reactants and products, suggesting that the destabilization due to the clustering of six rings around benzene is overestimated by computational calculations. The result for R3 is a bit strange, since it predicts a larger stabilization in **2** relative to 1,3,5-triphenylbenzene. We hypothesize that it can be related to some stabilization due to conjugation in 1,3,5-triphenylbenzene, which may be unaccounted for by the computational methods (such a conjugation effect should be disrupted in **2** due to the larger Ph-Ph dihedrals).

According to the literature, electronic structure analyses of aromatic interactions suggest that, although dispersion is the main stabilizing contribution for the total interaction energy, a smaller but still significant stabilization can come from electrostatic forces.^{48,51,54-56} In this way,

stating or implying that all the stabilization arising from aromatic interactions in the molecules of **1** and **2** comes from London dispersion can be misleading. In fact, without electronic structure analysis we cannot say exactly how much of the observed stabilization comes from London dispersion alone. Still, in the context of DFT calculations, it is well-known that methods without dispersion correction are virtually blind to aromatic $\pi\cdots\pi$ interactions (like the ones found in the molecules of **1** and **2**), and that inclusion of dispersion is capable of accounting for much of the interaction energy.⁵⁷⁻⁶² The characterization of such interactions in terms of electronic structure was already extensively investigated in the literature and is not the aim of this study. The aim of this study is to experimentally quantify the stabilization in the molecules of **1** and **2**, compare it with theoretical predictions, and indicate the most probable cause for this stabilization—aromatic interactions between the *ortho*-rings, which are mostly dispersive in nature.

Table 10 provides a complementary way to look at the thermochemical data; it shows the experimental and calculated DFT values of $\Delta_{\text{react}}H_{\text{m}}^0(\text{g})$ for the reactions representing the introduction of phenyl substituents into biphenyl to yield various polyphenylbenzenes. These homodesmotic reactions measure the total interaction enthalpy between all phenyl substituents in the selected molecules. For instance, the total interaction of the phenyl rings in penta- and hexaphenylbenzene is clearly repulsive; however, it is slightly stabilizing in 1,3,5-triphenylbenzene. The slightly endothermic reaction for **1** arises by compensation of the steric congestion in hexaphenylbenzene with stabilizing intramolecular interactions. This homodesmotic reaction shows that, although there are attractive forces within the molecule, repulsion due to steric crowding still prevails. The molecule **2** shows the strongest total interaction enthalpy, yet the contributions from its 1,2,3,5-tetraphenyl relationship must be discounted to make a realistic prediction of the magnitude of the intramolecular interactions.

Table 10. Experimental and calculated (PW6B95-D3(BJ)/6-311++G(2d,p) and [M052X-D3/6-311++G(2d,p)]) standard ($p^0 = 10^5$ Pa) molar enthalpies of reaction in the gas phase, $\Delta_{\text{react}}H_{\text{m}}^0(\text{g})$, at $T = 298.15$ K, for the homodesmotic reaction scheme used to evaluate the total substituent interaction enthalpy in selected polyphenylbenzenes.^a

Polyphenylbenzene	$\Delta_{\text{react}}H_{\text{m}}^0(\text{g}) / \text{kJ}\cdot\text{mol}^{-1}$		
	ΔH_{exptl}	$\Delta H_{\text{calcd}}^b$	$\Delta\Delta H^b$
1,3,5-Triphenylbenzene	-13 ± 3	-1 [-2]	12 [11]
1,2,3,5-Tetraphenylbenzene (7)	6 ± 5	10 [8]	4 [2]
Pentaphenylbenzene	18 ± 5	22 [17]	4 [-1]
Hexaphenylbenzene	18 ± 5	32 [26]	14 [8]
Decaphenylbiphenyl (1)	11 ± 9	38 [36]	27 [25]
Hexaphenylbiphenyl (2)	-19 ± 7	-14 [-10]	5 [9]

^a The following literature values of $\Delta_f H_{\text{m}}^0(\text{g})$, in $\text{kJ}\cdot\text{mol}^{-1}$, were used for the calculation of the tabulated $\Delta_{\text{react}}H_{\text{m}}^0(\text{g})$: benzene (82.9 ± 0.9),^{32,47} biphenyl (182.0 ± 0.7),³⁴ 1,3,5-triphenylbenzene (366.8 ± 4.9),³⁵ pentaphenylbenzene (596.5 ± 9.1),³¹ and hexaphenylbenzene (695.6 ± 8.3).⁴¹ ^b For each entry the PW6B95-D3(BJ) result is first and the M052X-D3 is right to it, in square brackets.

The experimental results of $\Delta_{\text{react}}H_{\text{m}}^0(\text{g})$ for the homodesmotic reactions presented in Tables 9 and 10 are reasonably well predicted by the theoretical DFT methods employed. However, they clearly overestimate the magnitude of destabilization in the two most congested molecules of the set (hexaphenylbenzene and **1**, Table 10), exposing the inadequacy of such methods for describing heavily crowded systems. The two DFT methods employed in Table 9 are among the most highly rated in the recent paper of Goerigk *et al.*,²⁶ and it is important to show how these methods compare with experiment. Grimme *et al.* claim in their review that “inclusion of these interactions in theoretical simulations is indispensable in order to reach chemical accuracy ($\sim 4 \text{ kJ}\cdot\text{mol}^{-1}$)”.²² Clearly, such accuracy has not yet been achieved and these

state-of-the-art DFT methods do not seem capable of fully describing some effects presented in relatively large aromatic systems like polyphenylbiphenyls. The results shown in Tables 9 and 10 also indicate that a careful balance of steric crowding is necessary to account for dispersive interactions if using homodesmotic schemes. This should be kept in mind when using dispersion-corrected DFT methods to estimate the magnitude of interactions with a significant contribution from London dispersion.

Conclusions

Recent computational studies utilizing dispersion-corrected DFT functionals suggest that the obviously crowded and seemingly strained decaphenylbiphenyl (**1**) is in fact not a high-energy molecule.³ In these calculations, the distortions in the structure due to steric repulsion are balanced by compensating attraction due mostly to London dispersion. In the present work, we determined the gas-phase enthalpies of formation of compound **1** and the closely related (and nearly as crowded) 2,2',4,4',6,6'-hexaphenylbiphenyl (**2**). The results clearly indicate that both molecules are strongly stabilized by intramolecular attraction between their many phenyl groups in the gas phase. The energetic analyses based on homodesmotic reactions show a surprising ability of crowded biphenyls to achieve significant enthalpic stabilization through intramolecular dispersion forces. Contrary to the usual expectations for very crowded molecular systems, aromatic interactions in the molecules of **1** and **2** are in fact capable of counterbalancing a great deal of steric repulsions. The total interaction energy within these molecules is as high as 30 kJ·mol⁻¹, making them considerably more stable than previously thought; a stabilization that is still underestimated by state-of-the-art DFT calculations.

Experimental

Decaphenylbiphenyl (1). In a modification of the procedure of Ogliaruso and Becker,¹ two identical reactions were performed. In each, diphenylbutadiyne (1.01 g, 5.00 mmol) and tetracyclone (5.8 g, 15 mmol) were mixed and then heated in a screw-capped Pyrex tube by placing it in a metal bath at 315 °C for 2 h. After cooling, the tubes were crushed, and the glass and organic solids were placed in a Soxhlet thimble. This material was extracted for 8 h with acetone in a Soxhlet extractor. After cooling, the acetone suspension (ca. 150 mL) was filtered, thus collecting 10.7 g of crude product.

This material was (mostly) dissolved in hot CHCl₃ (100 mL) in a beaker, and EtOH (100 mL) was added. The volume was reduced to 100 mL by boiling on a hot plate. After cooling, a grey solid was collected that was mostly **1**, but still contained substantial tetracyclone. This material was recrystallized from hot toluene (100 mL) to give **1** that was at least 95% pure as judged by TLC. Another recrystallization from hot toluene (50 mL) gave **1** (6.3 g) that was pure by TLC, but still pink (due to trace tetracyclone). A final recrystallization from hot toluene (40 mL) gave compound **1** (5.80 g) as a slightly off-white solid after drying at 110 °C under vacuum for 2 h.

The ¹³C NMR spectrum (CD₂Cl₂) of this material showed the presence of toluene. One of the crystals was submitted for X-ray analysis, and the resulting X-ray structure showed it to be the toluene solvate of **1** (**1**•C₇H₈), nearly isomorphous with the published² chloroform solvate (**1**•CHCl₃). A yield of 5.80 g of the toluene solvate corresponds to 5.77 mmol; thus, the yield was 57.4%. A later repetition of this procedure gave 7.0 g (70%) of **1**•C₇H₈.

Prior to the thermochemical experimental studies compound **1** was purified by three cycles of sublimation under reduced pressure. Each purification cycle consisted in heating the sample, under vacuum, at $T \approx 250$ °C to remove more volatile impurities, followed by heating at $T \approx 320$ °C, under vacuum, to sublime **1**.

Concerning the crystal structure determination for the novel *D*₂ polymorph (obtained by crystallization from 1,3,5-triisopropylbenzene), the low-quality data, often unavoidable in a

light-atom structure with a unit cell volume of $\sim 10^4 \text{ \AA}^3$, requires some additional comment. It could be the case that the D_2 structure is an illusion resulting from unrecognized disorder in the crystal. Indeed, it might be imagined that the overlap of the electron density due to a disordered superposition of two C_1 conformations might cause the boat-shaped central rings to appear flat and the observed structure to have approximate D_2 symmetry. However, while such a superposition might closely overlap the central rings, the two sets of peripheral phenyl groups would be displaced from each other, and it would then be impossible to refine those groups as a single set of rings on the periphery of the “ D_2 ” structure. Furthermore, even in the central rings, the superposition would be imperfect, and it would result in abnormally elongated thermal ellipsoids. No such features are observed in the structure, and hence there is no evidence for this kind of disorder. In addition, the final difference map for the refinement contains no peaks larger than $0.22 e\text{\AA}^{-3}$, far too small for there to be any unmodeled disorder. Finally, and perhaps more significantly, the D_2 conformation has already been observed in a simple derivative of decaphenylbiphenyl: 1,3-bis(nonaphenyl-3-biphenyl)benzene.⁵ This very large compound may be thought of as two decaphenylbiphenyl molecules that share one benzene ring. In this structure, which refines to a conventional $R(F)$ of 7.8%, both decaphenylbiphenyls adopt the D_2 conformation.

2,4,6-Triphenyliodobenzene (8). 2,4,6-Triphenylaniline (4.80 g, 15.0 mmol) was dissolved in dioxane (100 mL) in a 400-mL beaker. 10% aqueous H_2SO_4 (40 mL) was added, and the solution was cooled to 4 °C in an ice bath. A solution of NaNO_2 (1.04 g, 15.1 mmol) in water (20 mL) was added over 5 min, maintaining the temperature at or below 5 °C. This solution was stirred for 20 min, and then a solution of KI (5 g, 30 mmol) in water (30 mL) was added all at once. The resulting mixture was stirred in the ice bath for 60 min, then allowed to come to room temperature over 45 min, and then it was heated briefly to 70 °C.

After cooling, the mixture was poured into toluene and water (300 mL each) in a separatory funnel. After shaking, the organic layer was taken, and it was washed twice with a solution of NaOH and Na_2SO_3 . The organics were dried over Na_2SO_4 and then concentrated. This material

was chromatographed on a 2.5 cm x 30 cm silica gel column (solvent, 8:2 hexanes-toluene). Fractions of 125 mL were taken, and compound **8** was found in fractions 3 and 4. These were combined and concentrated to give compound **8** as a yellow oil (5.65 g, 13.1 mmol, 87%) that crystallized overnight.

The literature synthesis³⁷ of **8** does not specify a co-solvent. However, when the dioxane co-solvent is replaced by water, the yield of **8** is only 11%.

2,2',4,4',6,6'-Hexaphenylbiphenyl (2). In a modification of the procedure of Fujioka et al.,³⁷ compound **8** (2.88 g, 6.67 mmol) was mixed with Cu powder (4.0 g, 1 μm particle size) in a pear-shaped flask. The flask was placed in a metal bath at 280 °C for 1 h. The resulting solid was crushed and extracted repeatedly with toluene, with the total volume of the extracts being 200 mL. The extracts were filtered through celite, and concentration on a rotary evaporator gave a brown solid. A second reaction with compound **8** (5.65 g, 13.08 mmol) and Cu powder (7.1 g) was performed similarly.

The material from both runs was combined, partially dissolved in hexanes, and applied to a 2.5 cm x 30 cm silica gel column. The column was eluted with hexanes (2.5 L) followed by 9:1 hexanes-toluene (2.5 L), and fractions of 125 mL were collected. The unreacted **8** eluted with the hexanes. Fractions 28-33 contained pure compound **2** (0.59 g), and fractions 34-40 contained **2** that was perhaps 70% pure (0.35 g). However, due to its insolubility in the chromatography solvent mixture, much of the product remained on the column. Therefore, the column was stripped with CHCl_3 to give 1.28 g of material that was mostly **2** but contaminated with a variety of more polar compounds. The contents of the strip and fractions 34-40 were combined and recrystallized from CHCl_3 -EtOH to give material that was judged to be about 90-95% pure. This material was chromatographed on a second 2.5 cm x 30 cm silica gel column (solvent, 9:1 hexanes-toluene) which removed most, but not all polar contaminants. The product was recrystallized from CHCl_3 -EtOH to give 1.06 g of nearly pure **2**. This material was combined with the 0.59 g of **2** from the first column, and a final recrystallization was performed as follows. The combined products were dissolved in boiling CHCl_3 (50 mL), and EtOH (50 mL) was added

in portions while the solution continued to boil. With reduction of the volume, compound **2** began to precipitate, and when the volume had been reduced to 60 mL, the mixture was allowed to cool with further crystallization. The yield of **2** was 1.42 g (2.33 mmol, 23.6%) after drying overnight over P₂O₅.

Prior to the thermochemical experimental studies compound **2** was purified by two cycles of sublimation under reduced pressure. Each purification cycle consisted in heating the sample, under vacuum, at $T \approx 230$ °C to remove more volatile impurities, followed by heating at $T \approx 310$ °C, under vacuum, to sublime **2**.

1,2,3,5-Tetraphenylbenzene (7). A stirred suspension of 1-iodo-2,4,6-triphenylbenzene (**8**, 2.16 g, 5.00 mmol), benzenboronic acid (740 mg, 6.06 mmol), K₂CO₃ (13.8 g, 100 mmol) and Pd(PPh₃)₄ (640 mg, 0.55 mmol) in toluene (100 mL) was heated at reflux for 2 days under argon. Water (250 mL) was added, and the mixtures was extracted with CHCl₃ (3 × 100 mL). The combined organics were washed with brine and dried over Na₂SO₄, and the solvent was removed under vacuum. This resulting material was fractionated by silica gel chromatography (1:10 CH₂Cl₂-hexanes) to yield the target compound as a white solid. Then the white solid was recrystallized from CH₂Cl₂ to yield pure compound **7** (650 mg, 1.70 mmol, 34%), m.p. 221-223 °C (lit.⁶³ 224-226 °C).

Prior to the thermochemical experimental studies compound **7** was purified by two successive sublimations under reduced pressure at $T \approx 210$ °C. The final purity of **7** was checked by gas-liquid chromatography, by using an HP 4890 apparatus equipped with an HP-5 column [cross-linked diphenyl (5 %) and dimethylpolysiloxane (95 %)], which indicated a purity of 99.9 % (*m/m*).

Differential Scanning Calorimetry (DSC). The phase behavior and thermal study of compounds **1** and **2**, as well as their temperatures and standard molar enthalpies of melting, were measured in a heat flux differential scanning calorimeter (NETZSCH DSC 200 F3 MAIA). All measurements were performed under a constant flow of nitrogen (50 mL·min⁻¹), using a heating rate of 5 K min⁻¹, sealed aluminum crucibles with a small hole punctured on the top lid, and

samples of about 5 mg in each experiment. The temperature and heat flux scales were calibrated by measuring the temperature and the enthalpy of melting of some reference materials (*o*-terphenyl, benzoic acid, 1,3,5-triphenylbenzene, perylene, *p*-quaterphenyl).^{32,64} The compounds studied were measured using the same experimental procedure of the calibration runs.

High-precision heat capacity drop calorimetry. The heat capacities of the pure crystalline compounds **1** (C_1 and D_2 polymorphs) and **2** were measured at $T = (298.15 \pm 0.01)$ K by a high-precision heat capacity drop calorimeter, previously described in the literature.⁶⁵⁻⁶⁸ The calorimeter was calibrated with sapphire (α -Al₂O₃ pellets, NIST-RM 720) using the respective standard molar heat capacity at $T = 298.15$ K reported in the literature: $C_{p,m}^0(\alpha$ -aluminium oxide) = (79.03 ± 0.08) J·K⁻¹·mol⁻¹.⁶⁴ The calibration constant was found to be $\varepsilon = (6.647 \pm 0.019)$ W·V⁻¹. The precision and reproducibility of the apparatus for the measurements of the heat capacities of liquids and solids was evaluated before, using benzoic acid and hexafluorobenzene.⁶⁷ The uncertainties quoted are twice the standard deviation of the mean and include the calibration uncertainty.

Knudsen Effusion with Quartz Crystal Microbalance. The vapor pressures of compounds **1**, **2**, and **7** as a function of temperature were measured by a combined Knudsen/Quartz crystal effusion apparatus, described in detail elsewhere.^{69,70} This technique is based on the simultaneous gravimetric and quartz crystal microbalance mass loss detection, enabling the use of a temperature-step methodology, and having the advantages of small sample sizes and effusion times and the possibility of achieving temperatures up to 650 K. Like a typical Knudsen effusion experiment, the system is kept at high vacuum, enabling free effusion of the vapor from the Knudsen cell, which is kept in an oven at a fixed temperature. The experimental temperature (and pressure) ranges for the compounds studied were: 543 – 559 K (0.18 – 0.65 Pa) for **1**, 523 – 546 K (0.11 – 0.75 Pa) for **2**, and 429 – 453 K (0.09 – 1.00 Pa) for **7**.

Combustion Calorimetry. The standard molar enthalpies of combustion, $\Delta_c H_m^0$, at $T = 298.15$ K, for compounds **1**, **2**, and **7** were measured using an isoperibol mini-bomb combustion

calorimeter, described in detail elsewhere.⁷¹ The mini-bomb is made of stainless steel with 0.46 cm wall thickness and 18.2 cm³ of internal volume. The internal fittings located on the head of the mini-bomb (electrodes, crucible support and sheet) are all made of platinum. The program LABTERMO was used to compute the corrected adiabatic temperature change, ΔT_{ad} .⁷² The energy equivalent of the calorimeter, $\varepsilon(\text{calor}) / \text{J}\cdot\text{K}^{-1} = \{1947.28 \pm 0.09 (0.005\%)\}$, was obtained from 35 calibration experiments with benzoic acid (Calorimetric Standard NIST 39j) – the detailed results are presented in the ESI†. The densities of compounds **1**, **2**, and **7** were taken from the crystallographic data as 1.21 g·cm⁻³, 1.20 g·cm⁻³, and 1.20 g·cm⁻³,⁴⁵ respectively. The values of $(\partial u / \partial p)_T$ at $T = 298.15$ K, were assumed to be 0.2 J·g⁻¹·MPa⁻¹ – the corresponding energetic correction usually leads to negligible errors in the final combustion results.^{73,74} Standard state corrections were calculated for the initial and final states by the procedures given by Hubbard *et al.* and by Good and Scott.^{75,76} The relative atomic masses used were those recommended by IUPAC in 2007.⁷⁷

Computational Methodology. All density functional calculations were performed with Gaussian 16, revision C.01.³⁶ The built-in defaults for integral accuracy, wavefunction convergence, and gradient convergence were employed for all calculations. Potential minima were verified by analytical frequency calculations at the same level of theory as the geometry optimizations. The functional accessed by the Gaussian keyword PW6B95D3 is listed in this paper as PW6B95-D3(BJ) to reflect more clearly the composition of the method, which employs the D3(BJ) correction, not the D3 correction. Frequency scale factors were not considered for the calculation of enthalpies of reaction.

ASSOCIATED CONTENT

Data availability

Detailed description and tabulation of experimental methods and data, including differential scanning calorimetry, drop calorimetry, Knudsen effusion, combustion calorimetry, and UV-Vis spectroscopy; full tabulation of computational results and atomic coordinates of the calculated structures. This data is available in the ESI†.

Accession Codes

Four X-ray structures of compound **1** have been deposited with the CSD: CCDC 2207587 (*D*₂ polymorph), CCDC 2207588 (*C*₁ polymorph), CCDC 2207589 (toluene solvate), and CCDC 2207590 (nitrobenzene solvate). These data can be obtained free of charge via www.ccdc.cam.ac.uk/data_request/cif, or by emailing data_request@ccdc.cam.ac.uk, or by contacting The Cambridge Crystallographic Data Centre, 12 Union Road, Cambridge CB2 1EZ, UK; fax: +44 1223 336033.

Corresponding Author

Luís M. N. B. F. Santos, e-mail: lbsantos@fc.up.pt

Author Contributions

The manuscript was written with the contributions of all authors. All authors approved the final version of the manuscript. Carlos Lima: conceptualization, formal analysis, investigation, validation, visualization, and writing. Joel Mague: X-ray crystallography. Yuchen Du: organic synthesis. Robert Pascal: conceptualization, organic synthesis, computational studies, and writing. Luís Santos: formal analysis, methodologies, resources, software, visualization, and review.

Conflicts of interest

The authors declare no competing financial interest.

ACKNOWLEDGEMENTS

The authors thank the Portuguese Foundation for Science and Technology (FCT) for financial support for the project: CIQUP, Centro de Investigação em Química da Universidade do Porto (UIDB/00081/2020); IMS, Institute of Molecular Sciences (LA/P/0056/2020). CFRACL is financed by national funds through the FCT-I.P., in the framework of the execution of the program contract provided in paragraphs 4, 5, and 6 of art. 23 of Law no. 57/2016 of 29 August, as amended by Law no. 57/2017 of 19 July. The authors also thank the U.S. National Science Foundation, in the form of grants CHE-1762452 and MRI-1228232, for additional support for this project.

References and Notes

- (1) M. A. Ogliaruso and E. I. Becker, *J. Org. Chem.*, 1965, **30**, 3354-3360.
- (2) L. Tong, H. Lau, D. M. Ho and R. A. Pascal, Jr., *J. Am. Chem. Soc.*, 1998, **120**, 6000-6006.
- (3) Y. Du, J. T. Mague and R. A. Pascal, Jr., *Eur. J. Org. Chem.*, 2021, 3294-3302.
- (4) Y. Du, A. McSkimming, J. T. Mague and R. A. Pascal, Jr., *Chem. Eur. J.*, 2022, **28**, e202200931.
- (5) R. A. Pascal, Jr., N. Hayashi and D. M. Ho, *Tetrahedron*, 2001, **57**, 3549-3555.
- (6) X. Qiao, M. A. Padula, D. M. Ho, N. J. Vogelaar, C. E. Schutt and R. A. Pascal, Jr., *J. Am. Chem. Soc.*, 1996, **118**, 741-745.
- (7) Y. Xiao, J. T. Mague, J. P. Donahue, L. J. Wilson, C. M. Kraml and R. A. Pascal, Jr., *Chem. Eur. J.*, 2020, **26**, 8458-8464.
- (8) Y. Xiao, J. T. Mague, R. H. Schmehl, F. M. Haque and R. A. Pascal, Jr., *Angew. Chem. Int. Ed.*, 2019, **58**, 2831-2833.
- (9) C. H. Arnaud, *Chemical & Engineering News*, 2019, **97**.
- (10) A. J. Berresheim, M. Müller and K. Müllen, *Chem. Rev.*, 1999, **99**, 1747-1786.
- (11) P. Devibala, B. Balambiga, S. Noureen and S. Nagarajan, *RSC Adv.*, 2021, **11**, 11672-11701.
- (12) C. Dusold, B. Platzer, P. Haines, D. Reger, N. Jux, D. M. Guldi and A. Hirsch, *Chem. Eur. J.*, 2021, **27**, 1670-1679.
- (13) W. Soichi and K. Junji, *Chem. Lett.*, 2007, **36**, 590-591.
- (14) K. L. Mears and P. P. Power, *Acc. Chem. Res.*, 2022, **55**, 1337-1348.
- (15) D. J. Liptrot and P. P. Power, *Nat. Rev. Chem.*, 2017, **1**, 0004.
- (16) J. P. Wagner and P. R. Schreiner, *Angew. Chem. Int. Ed.*, 2015, **54**, 12274-12296.
- (17) S. Grimme and P. R. Schreiner, *Angew. Chem. Int. Ed.*, 2011, **50**, 12639-12642.
- (18) M. P. Mitoraj, M. G. Babashkina, A. Y. Isaev, Y. M. Chichigina, K. Robeyns, Y. Garcia and D. A. Safin, *Cryst. Growth Des.*, 2018, **18**, 5385-5397.

- (19) T. Li, P. W. Ayers, S. Liu, M. J. Swadley and C. Aubrey-Medendorp, *Chem. Eur. J.*, 2009, **15**, 361-371.
- (20) C. M. Roth, B. L. Neal and A. M. Lenhoff, *Biophys. J.*, 1996, **70**, 977-987.
- (21) R. W. Newberry and R. T. Raines, *ACS Chem. Biol.*, 2019, **14**, 1677-1686.
- (22) S. Grimme, A. Hansen, J. G. Brandenburg and C. Bannwarth, *Chem. Rev.*, 2016, **116**, 5105-5154.
- (23) U. Ryde, R. A. Mata and S. Grimme, *Dalton Trans.*, 2011, **40**, 11176-11183.
- (24) (a) A. D. Becke, *J. Chem. Phys.*, 1993, **98**, 5648-5652; (b) J. P. Perdew and Y. Wang, *Phys. Rev. B*, 1992, **45**, 13244-13249.
- (25) W. J. Hehre, L. Radom, P. v. R. Schleyer and J. A. Pople, *Ab Initio Molecular Orbital Theory*; John Wiley & Sons: New York, 1986; pp 63-100.
- (26) L. Goerigk, A. Hansen, C. Bauer, S. Ehrlich, A. Najibi and S. Grimme, *Phys. Chem. Chem. Phys.*, 2017, **19**, 32184-32215.
- (27) Y. Zhao, N. E. Schultz and D. G. Truhlar, *J. Chem. Theory and Comput.*, 2006, **2**, 364-382.
- (28) S. Grimme, J. Antony, S. Ehrlich and H. Krieg, *J. Chem. Phys.*, 2010, **132**, 154104.
- (29) Y. Zhao and D. G. Truhlar, *J. Phys. Chem. A*, 2005, **109**, 5656-5667.
- (30) A. D. Becke and E. R. Johnson, *J. Chem. Phys.*, 2005, **123**, 154101.
- (31) C. F. R. A. C. Lima, A. S. M. C. Rodrigues and L. M. N. B. F. Santos, *J. Phys. Chem. A*, 2017, **121**, 2475-2481.
- (32) M. V. Roux, M. Temprado, J. S. Chickos and Y. Nagano, *J. Phys. Chem. Ref. Data*, 2008, **37**, 1855.
- (33) H. Ha, J. A. Morrison and E. L. Richards, *J. Chem. Soc., Faraday Trans. 1*, 1976, **72**, 1051-1057.
- (34) R. D. Chirico, S. E. Knipmeyer, A. Nguyen and W. V. Steele, *J. Chem. Thermodyn.*, 1989, **21**, 1307-1331.
- (35) M. A. V. Ribeiro da Silva, L. M. N. B. F. Santos and L. M. S. S. Lima, *J. Chem.*

Thermodyn., 2010, **42**, 134-139.

(36) Gaussian 16, Revision C.01, M. J. Frisch, G. W. Trucks, H. B. Schlegel, G. E. Scuseria, M. A. Robb, J. R. Cheeseman, G. Scalmani, V. Barone, G. A. Petersson, H. Nakatsuji, X. Li, M. Caricato, A. V. Marenich, J. Bloino, B. G. Janesko, R. Gomperts, B. Mennucci, H. P. Hratchian, J. V. Ortiz, A. F. Izmaylov, J. L. Sonnenberg, D. Williams-Young, F. Ding, F. Lipparini, F. Egidi, J. Goings, B. Peng, A. Petrone, T. Henderson, D. Ranasinghe, V. G. Zakrzewski, J. Gao, N. Rega, G. Zheng, W. Liang, M. Hada, M. Ehara, K. Toyota, R. Fukuda, J. Hasegawa, M. Ishida, T. Nakajima, Y. Honda, O. Kitao, H. Nakai, T. Vreven, K. Throssell, J. A. Montgomery, Jr., J. E. Peralta, F. Ogliaro, M. J. Bearpark, J. J. Heyd, E. N. Brothers, K. N. Kudin, V. N. Staroverov, T. A. Keith, R. Kobayashi, J. Normand, K. Raghavachari, A. P. Rendell, J. C. Burant, S. S. Iyengar, J. Tomasi, M. Cossi, J. M. Millam, M. Klene, C. Adamo, R. Cammi, J. W. Ochterski, R. L. Martin, K. Morokuma, O. Farkas, J. B. Foresman and D. J. Fox, Gaussian, Inc., Wallingford CT, 2016.

(37) Y. Fujioka, S. Ozasa, K. Sato and E. Ibuki, *Chem. Pharm. Bull.*, 1985, **33**, 22-29.

(38) H. T. T. Nguyen, J. T. Mague, C. M. Kraml, N. Byrne and R. A. Pascal, Jr., *Tetrahedron*, 2019, **75**, 2778-2784.

(39) N. V. Sidgwick, *The Covalent Link in Chemistry*, Cornell University Press, Ithaca, NY, **1933**, p. 104.

(40) J. S. Chickos, *Thermochim. Acta*, 1998, **313**, 19-26.

(41) C. F. R. A. C. Lima, M. A. A. Rocha, A. Melo, L. R. Gomes, J. N. Low and L. M. N. B. F. Santos, *J. Phys. Chem. A*, 2011, **115**, 11876-11888.

(42) I. M. Alecu, J. Zheng, Y. Zhao and D. G. Truhlar, *J. Chem. Theory Comput.*, 2010, **6**, 2872-2887.

(43) E. Gagnon, T. Maris, P. M. Arseneault, K. E. Maly and J. D. Wuest, *Cryst. Growth Des.*, 2010, **10**, 648-657.

(44) M. A. V. Ribeiro da Silva, L. M. N. B. F. Santos and L. M. S. S. Lima, *J. Chem. Thermodyn.*, 2008, **40**, 375-385.

- (45) C. P. G. Rühle, J. Niere, P. D. Morrison, R. C. Jones, T. Caradoc-Davies, A. J. Canty, M. G. Gardiner, V.-A. Tolhurst and P. J. Marriott, *Anal. Chem.*, 2010, **82**, 4501-4509.
- (46) CODATA Key Values for Thermodynamics; J. D. Cox, D. D. Wagman and V. A. Medvedev, Eds.; Hemisphere: New York, 1989.
- (47) C. G. Kruif, *J. Chem. Thermodyn.*, 1980, **12**, 243-248.
- (48) C. F. R. A. C. Lima, M. A. A. Rocha, L. R. Gomes, J. N. Low, A. M. S. Silva and L. M. N. B. F. Santos, *Chem. - Eur. J.*, 2012, **18**, 8934-8943.
- (49) M. O. Sinnokrot and C. D. Sherrill, *J. Phys. Chem. A*, 2006, **110**, 10656-10668.
- (51) C. A. Hunter, K. R. Lawson, J. Perkins, C. J. Urch, R. S. Mulliken, L. J. Andrews, J. Landauer, H. McConnell, M. G. Lawrey, H. McConnell et al., *J. Chem. Soc. Perkin Trans. 2*, 2001, **72**, 651-669.
- (51) S. Tsuzuki, Interactions with Aromatic Rings. In *Struct. Bonding* (Berlin); Springer-Verlag: Berlin/Heidelberg, 2005; Vol. 115, pp 149-193.
- (52) D. B. Ninković, J. P. B. Filipović, M. B. Hall, E. N. Brothers and S. D. Zarić, *ACS Cent. Sci.*, 2020, **6**, 420-425.
- (53) J. Hwang, B. E. Dial, P. Li, M. E. Kozik, M. D. Smith and K. D. Shimizu, *Chem. Sci.*, 2015, **6**, 4358-4364.
- (54) M. O. Sinnokrot and C. D. Sherrill, *J. Phys. Chem. A*, 2004, **108**, 10200-10207.
- (55) S. Tsuzuki, K. Honda, T. Uchimaru, M. Mikami and K. Tanabe, *J. Am. Chem. Soc.*, 2002, **124**, 104-112.
- (56) E. C. Lee, D. Kim, P. Jurečka, P. Tarakeshwar, P. Hobza and K. S. Kim, *J. Phys. Chem. A*, 2007, **111**, 3446-3457.
- (57) Y. Zhao and D. G. Truhlar, *Theor. Chem. Acc.*, 2007, **120**, 215-241.
- (58) S. Grimme, *WIREs Comput. Mol. Sci.*, 2011, **1**, 211-228.
- (59) N. Marom, A. Tkatchenko, M. Rossi, V. V. Gobre, O. Hod, M. Scheffler and L. Kronik, *J. Chem. Theory Comput.*, 2011, **7**, 3944-3951.
- (60) S. Ehrlich, J. Moellmann and S. Grimme, *Acc. Chem. Res.*, 2013, **46**, 916-926.

- (61) R. Podeszwa and K. Szalewicz, *J. Chem. Phys.*, 2012, **136**, 161102.
- (62) J. Antony and S. Grimme, *Phys. Chem. Chem. Phys.*, 2006, **8**, 5287-5293.
- (63) G. F. Woods, J. E. Swenarton and R. B. Isaacson, *J. Org. Chem.*, 1961, **26**, 309-312.
- (64) R. Sabbah, A. Xu-wu, J. S. Chickos, M. L. Leitão, M. V. Roux and L. A. Torres, *Thermochim. Acta*, 1999, **33**, 93-204.
- (65) J. Konicek, I. Wadsö and J. Suurkuus, *Chem Scripta*, 1971, **1**, 217-220.
- (66) J. Suurkuus and I. Wadsö, *J. Chem. Thermodyn.*, 1974, **6**, 667-679.
- (67) L. M. N. B. F. Santos, M. A. A. Rocha, A. S. M. C. Rodrigues, V. Štejfa, M. Fulem and M. Bastos, *J. Chem. Thermodyn.*, 2011, **43**, 1818-1823.
- (68) C. E. S. Bernardes, L. M. N. B. F. Santos and M. E. Minas da Piedade, *Meas. Sci. Tech.*, 2006, **17**, 1405-1408.
- (69) L. M. N. B. F. Santos, L. M. S. S. Lima, C. F. R. A. C. Lima, F. D. Magalhães, M. C. Torres, B. Schröder and M. A. V. Ribeiro da Silva, *J. Chem. Thermodyn.*, 2011, **43**, 834-843.
- (70) M. Fulem, K. Růžička, C. Červinka, M. A. A. Rocha, L. M. N. B. F. Santos and R. F. Berg, *J. Chem. Thermodyn.*, 2013, **57**, 530-540.
- (71) M. A. V. Ribeiro da Silva, G. Pilcher, L. M. N. B. F. Santos and L. M. S. S. Lima, *J. Chem. Thermodyn.*, 2007, **39**, 689-697.
- (72) L. M. N. B. F. Santos, M. T. Silva, B. Schröder and L. Gomes, *J. Therm. Anal. Calorim.*, 2007, **89**, 175-180.
- (73) W. H. Johnson, *J. Res. Natl. Bur. Stand.*, 1975, **79A**, 425-429.
- (74) E. W. Washburn, *J. Res. Natl. Bur. Stand.*, 1933, **10**, 525-558.
- (75) W. N. Hubbard, D. W. Scott and G. Waddington, In *Experimental Thermochemistry*; F. D. Rossini, Ed.; Interscience: New York, 1956; Vol. 1, Chapter 5.
- (76) W. D. Good and D. W. Scott, In *Experimental Thermochemistry*; H. A. Skinner, Ed.; Interscience: New York, 1962; Vol. 2, Chapter 2.
- (77) M. E. Wieser and T. B. Coplen, *Pure Appl. Chem.*, 2010, **83**, 359-396.